NASA Technical Memorandum 88315

Tilt-Rotor Flutter Control in Cruise Flight

Ken-ichi Nasu

December 1986

National Aeronautics and
Space Administration

NASA Technical Memorandum 88315

Tilt-Rotor Flutter Control in Cruise Flight

Ken-ichi Nasu, Ames Research Center, Moffett Field, California

December 1986

National Aeronautics and
Space Administration

Ames Research Center
Moffett Field, California 94035

TILT-ROTOR FLUTTER CONTROL IN CRUISE FLIGHT

Ken-ichi Nasu*
Ames Research Center

SUMMARY

Tilt-rotor flutter control under cruising operation is analyzed. The rotor model consists of a straight fixed wing, a pylon attached to the wingtip, and a three-bladed rotor. The wing is cantilevered to the fuselage and is allowed to bend forward and upward. It also has a torsional degree of freedom about the elastic axis. Each rotor blade has two bending degrees of freedom. Feedback of wingtip velocity and acceleration to cyclic pitch is investigated for flutter control, using strip theory and linearized equations of motion. To determine the feedback gain, an eigenvalue analysis is performed. A second, independent, timewise calculation is conducted to evaluate the control law while employing more sophisticated aerodynamics. The effectiveness of flutter control by cyclic pitch change was confirmed.

NOMENCLATURE

A	blade aspect ratio
A^i_{kj}	defined in equations (55) through (61) for $k = 1, \ldots, 7$
A_W	wing aspect ratio
a_e	position of elastic axis from leading edge, nondimensionalized by wing chord
a_i, a_j	ith, jth generalized coordinate for wing deformation
a_{jk}	kth generalize coordinate for the wing's jth deformation mode: $\dot{a}_j, \dot{a}_j, a_j, \dot{a}_j, a_j$ for $k = 1, \ldots, 5$, respectively
a_w	position of pitch axis from leading edge, nondimensionalized by wing chord

* National Research Council Research Associate

$\mathbf{B}^c$	matrix, containing virtual work on blade caused by lateral cyclic pitch
$\mathbf{B}^s$	matrix, containing virtual work on blade caused by longitudinal cyclic pitch
C	Theodorsen function
C_d	sectional drag coefficient
$C_{l\alpha}$	sectional lift slope
C_m	sectional pitching moment coefficient
c_g	position of center of gravity of wing from leading edge, nondimensionalized by wing chord
c	blade chord
c_w	wing chord
$\mathbf{D}$	physical state equation matrix, defined in equations (112) and (114), and in appendix B
d	drag per unit length
d_w	wing drag per unit length
$\mathbf{E}^n$	physical equation matrix for the nth order time derivative of state vector $\mathbf{X}$; defined in equations (112) and (113), and in appendix B
EI_B	blade bending stiffness perpendicular to chordline
EI_C	blade bending stiffness along chordline
EI_{BW}	wing bending stiffness perpendicular to chordline
EI_{CW}	wing bending stiffness along chordline
F_i	virtual work on wing caused by blade loading through the ith deformation mode
f_m	wing torsional moment around the elastic axis (positive nose up)
f_x	wing loading in x-direction per unit length (positive upward)
f_z	wing loading in z-direction per unit length (positive forward)
G_i	virtual work on wing caused by wing loading through the ith deformation mode
GJ_W	wing torsional rigidity
G^i_{W1}	constant virtual work component on the wing, defined by equation (105)
G^i_{Wkj}	virtual work component on the wing caused by the wing's jth deformation mode in term of generalized coordinates a_j and $\dot{a}_j$ for $k = 2, 3$, respectively; defined by equations (106) and (107)
h	mast height; distance between rotor and the wing elastic axis
$\mathbf{I}_9$	unit matrix of order nine
I_B	blade flapping mass moment of inertia

I_0^i	constant (independent of generalized coordinates) virtual work component on blade caused by the blade's jth deformation mode; defined in equation (87)
I_{Bk}^i	virtual work components on blade caused by the blade's jth deformation mode in terms of generalized coordinates $(a_j k)$; defined in equations (93) through (97) for $k = 1, \ldots, 5$
I_C^i	virtual work component on blade defined in equation (98)
I_S^i	virtual work component on blade defined in equation (99)
I_{Wk}^i	virtual work components on blade caused by the wing's jth deformation mode in terms of generalized coordinates $(q_j k)$; defined in equations (88) through (92) for $k = 1, \ldots, 5$
I_{pp}	pylon pitching mass moment of inertia about the intersection of pylon and wing elastic axis
I_{pr}	pylon rolling mass moment of inertia about the intersection of pylon and wing elastic axis
I_{py}	pylon yawing mass moment of inertia about the intersection of pylon and wing elastic axis
I_W	wing mass moment of inertia around elastic axis per unit length
K_{Bkj}^i	virtual work component on wing caused by the blade's ith deformation mode in terms of generalized coordinates $q_j k$; defined in appendix A for $k = 1, \ldots, 5$
K_C^i	virtual work component on wing caused by cyclic pitch (cosine term); defined in appendix A
K_S^i	virtual work component on wing caused by cyclic pith (sine term); defined in appendix A
K_{Wkj}^i	virtual work component on wing caused by the wing's ith deformation mode in terms of generalized coordinates $q_j k$; defined in appendix A for $k = 1, \ldots, 5$
K_0^i	constant virtual work component defined in appendix A
$K_{-cd}, K_{-cdd},$ K_{-sd}, K_{-sdd}	constants, associated with first, second order time derivatives of wing deformation variables - (u_w, w_w, p_w), for lateral and longitudinal cyclic pitch; equations (116), (117)
L	wing semispan
l	lift per unit length
l_b	blade lift per unit length
l_k	harmonic component of lift
l_s	steady component of lift
l_v	virtual mass component of lift
l_w	wing lift per unit length

M	Mach number
M_B	blade mass
M_P	pylon mass
m	blade mass per unit length
m_e	wing torsional (pitching) moment around elastic axis per unit length
m_k	harmonic component of wing pitching moment
m_s	steady component of wing pitching moment
m_v	virtual-mass component of wing pitching moment
m_w	wing mass per unit length
N	number of blades
N_{pi}	wingtip pitch angle caused by ith deformation mode; equation (44)
N_{ri}	wingtip roll angle caused by ith deformation mode; equation (45)
N_{yi}	wingtip yaw angle caused by ith deformation mode; equation (43)
P_n^i	virtual work done by the forces on nth blade through the ith deformation mode
$\mathbf{P}$	wingtip deformation matrix, containing P_{Wi} terms, equation (126)
P_{Wi}	ith mode of wing torsion deformation p_w
p_w	wing torsional deformation around the elastic axis (positive nose up)
$p_{\theta n}$	nth blade loading in the rotational plane (positive rotational direction)
p_{zn}	nth blade loading out of rotational plane (positive forward)
Q_{kj}^i	defined in equations (49) through (53) for $k = 1, \ldots, 5$
q_{jk}	blade generalized coordinate for jth deformation mode: $\dot{q}_{j0}, \dot{q}_{js}, q_{jc}, \dot{q}_{jc}, q_{js}$ for $k = 1, \ldots, 5$, respectively
q_{ni}	ith generalized coordinate for nth rotor blade deformation
R	rotor radius
R_C	radius at airfoil inboard section (rotor cut-out)
r	rotor blade radial position from center of rotation
r_x	pylon displacement in x-direction (positive upward)
r_z	pylon displacement in z-direction (positive forward)
$\mathbf{S}$	stability matrix, equation (127)
S_{Bkj}	air loading component caused by blade's jth deflection mode in terms of generalized coordinates (q_j); defined in equations (76) through (80) for $k = 1, \ldots, 5$
S_w	wing area
S_{Wkj}	air loading component caused by wing's jth deflection mode in terms of generalized coordinates (a_j); defined in equations (81) through (85) for $k = 1, \ldots, 5$

S_α	static mass moment of wing around elastic axis per unit length, $S_\alpha = m_w e_w (a_e - c_g)$
T	transformation matrix defined in equation (30)
t	time
U	air velocity at blade section
U_{Wi}	ith mode of wing deformation u_w
u_s	induced velocity
u_t	blade tip velocity
u_w	wing upward deformation
$\mathbf{V}$	wingtip deformation matrix, containing V_{Wi} terms, equation (124)
V	airplane cruise velocity
V_i	ith mode of blade deformation v_n
V_R	air velocity at rotor blade section
V_{Wi}	ith mode of wing deformation v_w
V_{0i}	defined in equation (7)
V_{1i}	defined in equation (8)
v_d	downwash caused by wing
v_{in}	in plane air-velocity component relative to blade caused by wing deformation
v_n	nth blade inplane deformation (positive in rotational direction)
v_{out}	out-of-plane air-velocity component relative to blade caused by wing deformation
$\dot{v}_p$	blade deformation velocity perpendicular to $\vec{r} \times \vec{\Omega} + \vec{V}$
v_w	wing deformation in x-direction (positive upward)
$\mathbf{W}$	wingtip deformation matrix, containing W_{Wi} terms, equation (125)
W_i	ith mode of blade deformation w
W_{Wi}	ith mode of wing deformation w_w
W_{0i}	defined in equation (9)
W_{1i}	defined in equation (10)
w_n	nth blade out-of-plane deformation (positive forward)
w_w	wing deformation in z-direction (positive forward)
$\mathbf{X}$	state vector, defined in equation (115)
X_i	wingtip x-displacement caused by ith mode; equation (41)
y	wing spanwise position from aircraft symmetry plane
Z_i	wingtip z-displacement caused by ith mode; equation (42)
α	angle of attack
α_G	geometric angle of attack
Δv	induced velocity
$\Delta\gamma$	circulation

η	correction factor, given by $\eta_1\eta_2$
η_1	aspect ratio correction factor
η_2	correction factor for spanwise location of vortex trailing
θ	blade pitch angle
θ_c	lateral cyclic pitch
θ_n	pitch control input (collective and cyclic) for nth blade
θ_s	longitunal cyclic pitch
θ_w	wing pitch angle
$\hat{\theta}_0$	collective pitch
ρ	air density
ν_p	pylon pitching angle (positive nose up)
ν_r	pylon rolling angle (positive clockwise)
ν_y	pylon yawing angle (positive counterclockwise)
ϕ	inflow angle
ϕ_w	inclination of wing lift
ψ_n	azimuth angle of nth blade
Ω	rotor rotational velocity
ω_i	rotor ith modal natural frequency
ω_{wi}	wing ith modal natural frequency
$(\ )^t$	transposed matrix
$\bar{(\ )}$	complex variable
$\dot{(\ )}$, $\ddot{(\ )}$	time derivative $\frac{\partial}{\partial t}$, $\frac{\partial^2}{\partial t^2}$
$(\ )'$, $(\ )''$, $(\ )'''$	spanwise derivative $\frac{\partial}{\partial y}$, $\frac{\partial^2}{\partial y^2}$, $\frac{\partial^3}{\partial y^3}$, or radius-wise derivative $\frac{\partial}{\partial r}$, $\frac{\partial^2}{\partial r^2}$, $\frac{\partial^3}{\partial r^3}$
$(\ )_{cos}$, $(\ )_c$	$cos(\psi_n)$ term; cyclic pitch
$(\ )_i$, $(\ )_j$	deformation mode i, j
$(\ )_n$	nth rotor blade
$(\ )_o$, $(\ )_0$	constant term, i.e., independent of ψ_n; collective pitch
$(\ )_{sin}$, $(\ )_s$	$sin(\psi_n)$ term; cyclic pitch
$(\ )_{tip}$	wing tip
$\mathbf{0}_9$	zero square matrix of order nine

Superscript

c	lateral cyclic pitch
I	inverse matrix
s	longitudinal cyclic pitch
0	collective pitch

Subscripts

B, b	blade
c	lateral cyclic pitch
d	indicates constant associated with first order time derivative
dd	indicates constant associated with second order time derivative
i, j, k	indices
p	wing torsional deformation
s	longitudinal cyclic pitch
tip	wingtip
u	wing upward deformation
W, w	wing
w	in K-constants: wing chordwise deformation
x	in x-direction
z	in z-direction

INTRODUCTION

The tilt-rotor aircraft is one of the promising transportation systems of the near future. It realizes a unique flight capability with its configuration. In the current trend toward using active control systems to widen the allowable flight conditions in fixed-wing aircraft or in conventional rotorcraft, it is of interest to consider active controls for the tilt-rotor aircraft to expand its flight envelope, maneuverabily and versatility. Active control systems for rotorcraft have been studied for years, but until recently almost all such studies dealt with active control systems to reduce the vehicle's gust response. It may be said that those studies have been aimed at coping with unusual phenomena which occur under normal operating conditions. In contrast, the objective of the flutter control studies is to enable the aircraft or rotorcraft to fly at higher speeds, to dive more steeply, or to allow a reduction of structural weight. In this report, tilt-rotor flutter control using rotor cyclic pitch is treated using the governing equations of reference 1. Determination of the control law is based on a harmonic method using wing tip deflection as the feedback. The control law determined in this way is further examined by timewise calculation using the local circulation method, where more precise aerodynamic theories are involved (references 2 through 5).

TILT-ROTOR MODEL AND EQUATIONS OF MOTION

Figure 1 illustrates the tilt-rotor model considered here, which consists of a cantilevered wing, a pylon, and rotor blades. This model is for airplane cruise mode, which is the major concern in this report. Operation in helicopter mode or tranition mode is not considered. The wing has one torsional and two bending degrees of freedom about the elastic axis. Wing dihedral angle and sweep angle are not considered. The pylon is rigidly attached at the wingtip, its direction is assumed to be parallel to the cruising velocity, and at the end of the pylon is a hingeless three-bladed rotor. The rotor blade also has a straight elastic axis, with elastic lead-lag and flapping degrees of freedom. In both the wing and the rotor blade, one of the principal elastic axes for bending coincides with the zero-lift- or chord-line. Aircraft motion is not considered. Since the wing is cantilevered to the fuselage, wing antisymmetric motion is also neglected (reference 6).

One coordinate system is assumed fixed to the aircraft (figure 2); consequently, it is an inertia system. The X-axis is directed upward. The Y-axis coincides with the wing elastic axis. The Z-axis is directed forward. The aircraft cruising velocity V is in the Z direction, but the wing-elastic principal axes do not necessarily coincide with the X- and Z-axes. The origin of this coordinate system is located at the intersection of wing elastic axis and aircraft-symmetry plane. The rotor is located at a distance h forward from the wing elastic axis at the wingtip.

Figure 3 shows the wing and blade deflections. The wing deflection is expressed in the X- and Z-direction, u_w and w_w (positive upward and forward, respectively), and torsion about the elastic axis, p_w (positive nose up). The deflected position of the pylon root is described as $(u_{w,tip},\ L,\ w_{w,tip})$ or $(r_x,\ L,\ r_z)$. The pylon direction is given by yawing, pitching, and rolling angles that are denoted by ν_y, ν_p, and ν_r, respectively, which are equal to $w'_{w,tip}$, $p_{w,tip}$ and $-u'_{w,tip}$, respectively. The rotor rotates clockwise for an observer looking forward and the nth rotor blade azimuth angle ψ_n is measured from the vertical position. This reference direction moves with the pylon rolling motion, so the blade azimuth angle in reference to the inertia system is given by $\psi_n + \nu_r$ (figure 4). Blade deflection is expressed in terms of in-the-rotational-plane v_n (positive in the rotational direction) and out-of-the-rotational-plane w_n (positive forward) bending.

The blade and wing deflections are described in series of natural modes (reference 7).

$$v_n = \sum_i q_{ni}(t) V_i(r) \tag{1}$$

$$w_n = \sum_i q_{ni}(t) W_i(r) \tag{2}$$

$$u_w = \sum_i a_i(t) U_{Wi}(y) \tag{3}$$

$$w_w = \sum_i a_i(t) W_{Wi}(y) \tag{4}$$

$$p_w = \sum_i a_i(t) P_{Wi}(y) \tag{5}$$

The equations of motion for the blade and wing generalized coordinates q_{ni} and a_i are taken from reference 1.

The equations for the deformation of the nth rotor blade are

$$\begin{aligned}\ddot{q}_{ni} + \omega_i^2 q_{ni} + V_{1i}\ddot{\nu}_r - V_{0i}\left(\frac{\ddot{r}_x}{R} + \frac{h}{R}\ddot{\nu}_p\right)\sin\psi_n + W_{0i}\frac{\ddot{r}_z}{R} - \frac{h}{R}V_{0i}\ddot{\nu}_y\cos\psi_n \\ + W_{1i}\ddot{\nu}_y\sin\psi_n - W_{1i}\ddot{\nu}_p\cos\psi_n + 2\Omega W_{1i}\dot{\nu}_y\cos\psi_n + 2\Omega W_{1i}\dot{\nu}_p\sin\psi_n \\ = P_n^i\end{aligned} \tag{6}$$

$$V_{0i} = R\int_0^R m V_i\, dr \tag{7}$$

$$V_{1i} = \int_0^R m r V_i\, dr \tag{8}$$

$$W_{0i} = R\int_0^R m W_i\, dr \tag{9}$$

$$W_{1i} = \int_0^R m r W_i\, dr \tag{10}$$

where P_n^i is virtual work done by the forces on the nth blade through the ith deformation mode .

For wing deformation the equation is

$$\begin{aligned}\ddot{a}_i + \omega_{wi}^2 a_i + I_B N\Omega(W'_{Wi,tip}\dot{\nu}_p - P_{Wi,tip}\dot{\nu}_y) \\ + \sum_{n=1}^{N}\sum_j\left\{(-V_{1j}U'_{Wj,tip} + W_{0j}\frac{W_{Wj,tip}}{R})\ddot{q}_{nj}\right. \\ \left. + \left[-V_{0j}(\frac{U_{Wj,tip}}{R} + \frac{h}{R}P_{Wj,tip}) + W_{1j}W'_{Wj,tip}\right]\ddot{q}_{nj}\sin\psi_n\right.\end{aligned}$$

$$
\begin{aligned}
&- (V_{0j}\frac{h}{R} + W_{1j}P_{Wj,tip})\ddot{q}_{nj}\cos\psi_n \\
&- 2\Omega V_{0j}(\frac{U_{Wj,tip}}{R} + \frac{h}{R}P_{Wj,tip})\dot{q}_{nj}\cos\psi_n \\
&+ 2\Omega(\frac{h}{R}V_{0j}W'_{Wj,tip})\dot{q}_{nj}\sin\psi_n \\
&+ \Omega^2(\frac{h}{R}V_{0j}W'_{Wj,tip} - W_{1j}P_{Wj,tip})q_{nj}\cos\psi_n \\
&+ \Omega^2\left[V_{0j}(\frac{U_{Wj,tip}}{R} + \frac{h}{R}P_{Wj,tip}) + W_{1j}W'_{Wj,tip}\right]q_{nj}\sin\psi_n\Bigg\} \\
&= F_i + G_i
\end{aligned}
\tag{11}
$$

where F_i and G_i are the virtual work done by forces on blade and wing, respectively, through the ith deformation mode. Natural modes V_i, W_i, U_{Wi}, W_{Wi}, and P_{Wi}, and corresponding frequencies ω_i and ω_{wi} satisfy the following equations of motion and boundary and normalization conditions.

Equations of motion for the natural modes of vibration are

Blade:

$$
\begin{aligned}
&\frac{d^2}{dr^2}\left[\left(EI_C\sin^2\theta + EI_B\cos^2\theta\right)\frac{d^2W_i}{dr^2}\right] \\
&\quad + \frac{d^2}{dr^2}\left[\left(EI_C - EI_B\right)\sin^2\theta\cos^2\theta\frac{d^2V_i}{dr^2}\right] \\
&\quad - \frac{d}{dr}\left(\int_r^R mx\,dx\frac{dV_i}{dr}\right) - \omega_i^2 mW_i = 0
\end{aligned}
\tag{12}
$$

$$
\begin{aligned}
&\frac{d^2}{dr^2}\left[\left(EI_C\cos^2\theta + EI_B\sin^2\theta\right)\frac{d^2V_i}{dr^2}\right] \\
&\quad + \frac{d^2}{dr^2}\left[\left(EI_C - EI_B\right)\sin^2\theta\cos^2\theta\frac{d^2W_i}{dr^2}\right] \\
&\quad - \frac{d}{dr}\left(\int_r^R mx\,dx\frac{dW_i}{dr}\right) - m(\omega_i^2 + \Omega^2)V_i = 0
\end{aligned}
\tag{13}
$$

Wing:

$$
\frac{d^2}{dy^2}\left[\left(EI_{CW}\sin^2\theta_w + EI_{BW}\cos^2\theta_w\right)\frac{d^2U_{Wi}}{dy^2}\right]
$$

$$+\frac{d^2}{dy^2}\left[(EI_{CW}-EI_{BW})\sin^2\theta_w\cos^2\theta_w\frac{d^2W_{Wi}}{dy^2}\right]$$
$$-\omega_{wi}^2(m_w-S_\alpha P_{Wi})=0 \tag{14}$$

$$\frac{d^2}{dy^2}\left[(EI_{CW}\cos^2\theta_w+EI_{BW}\sin^2\theta_w)\frac{d^2W_{Wi}}{dy^2}\right]$$
$$+\frac{d^2}{dy^2}\left[(EI_{CW}-EI_{BW})\sin^2\theta_w\cos^2\theta_w\frac{d^2U_{Wi}}{dy^2}\right]$$
$$-\omega_{wi}^2 m_w W_{Wi}=0 \tag{15}$$

$$\frac{d}{dy}\left(GJ_W\frac{dP_{Wi}}{dy}\right)-\omega_{wi}^2(I_W P_{Wi}+S_\alpha U_{Wi})=0 \tag{16}$$

The equations for the boundary conditions are

At the bladetip:

$$V_i''=0,\ V_i'''=0,\ W_i''=0,\ W_i'''=0 \tag{17}$$

At the bladeroot:

$$V_i=0,\ V_i'=0,\ W_i=0,\ W_i'=0 \tag{18}$$

At the wingroot:

$$U_{Wi}=0,\ U_{Wi}'=0,\ W_{Wi}=0,\ W_{Wi}'=0,\ P_{Wi}=0 \tag{19}$$

At the wingtip

$$M_P\ddot{r}_x-\frac{\partial}{\partial y}\left[(EI_{CW}\sin^2\theta_w+EI_{BW}\cos^2\theta_w)\frac{\partial^2U_{Wi}}{\partial y^2}\right]$$
$$-\frac{\partial}{\partial y}\left[(EI_{CW}-EI_{BW})\sin\theta_w\cos\theta_w\frac{\partial^2W_{Wi}}{\partial y^2}\right]$$
$$+NM_B\ddot{r}_x+NM_Bh\ddot{\nu}_p=0 \tag{20}$$

$$M_P\ddot{r}_z-\frac{\partial}{\partial y}\left[(EI_{CW}\cos^2\theta_w+EI_{BW}\sin^2\theta_w)\frac{\partial^2U_{Wi}}{\partial y^2}\right]$$

$$- \frac{\partial}{\partial y}\left[(EI_{CW} - EI_{BW})\sin\theta_w \cos\theta_w \frac{\partial^2 W_{Wi}}{\partial y^2}\right]$$
$$+ NM_B \ddot{r}_z = 0 \tag{21}$$

$$I_{py}\ddot{\nu}_y + (EI_{CW}\cos^2\theta_w + EI_{BW}\sin^2\theta_w)\frac{\partial^2 U_{Wi}}{\partial y^2}$$
$$+ (EI_{CW} - EI_{BW})\sin\theta_w\cos\theta_w \frac{\partial^2 W_{Wi}}{\partial y^2}$$
$$+ NM_B h^2 \ddot{\nu}_y + \frac{N}{2} I_B \ddot{\nu}_y = 0 \tag{22}$$

$$I_{pp}\ddot{\nu}_p + GJ_W \frac{\partial P_{Wi}}{\partial y} + NM_B h^2 \ddot{\nu}_p + \frac{N}{2} I_B \ddot{\nu}_p = 0 \tag{23}$$

$$I_{pr}\ddot{\nu}_r - (EI_{CW}\sin^2\theta_w + EI_{BW}\cos^2\theta_w)\frac{\partial^2 U_{Wi}}{\partial y^2}$$
$$- (EI_{CW} - EI_{BW})\sin\theta_w\cos\theta_w \frac{\partial^2 W_{Wi}}{\partial y^2} + NI_B \ddot{\nu}_r = 0 \tag{24}$$

The equations for the normalization conditions are

Blade:

$$\int_0^R m(V_i^2 + W_i^2)\, dr = 1 \tag{25}$$

Wing:

$$\int_0^L \left[m_w\left(U_{Wi}^2 + W_{Wi}^2\right) + I_W P_W^2 + 2S_\alpha U_{Wi} P_{Wi}\right] dy$$
$$+ \left[M_P\left(U_{Wi}^2 + W_{Wi}^2\right) + I_{py}\left(W'_{Wi}\right)^2 + I_{pp}P_{Wi}^2 + I_{pr}\left(U'_{Wi}\right)^2\right]_{y=L}$$
$$+ NM_B\left[\left(U_{Wi} + hP_{Wi}\right)^2 + h^2\left(W'_{Wi}\right)^2 + W_{Wi}^2\right]_{y=L}$$
$$+ \frac{NI_B}{2}\left[2\left(U'_{Wi}\right)^2 + \left(W'_{Wi}\right)^2 + P_{Wi}^2\right]_{y=L} = 1 \tag{26}$$

These equations do not have the expressions for the virtual work terms P_n^i, F_i and G_i. These virtual work terms are directly related to the air loading and can be calculated under

various assumptions such as quasi-steady or unsteady aerodynamics, lifting line theory, or lifting surface theory. There are many possible options in calculating aerodynamic loading, and some of them restrict the validity of the final equations. For that reason, details of the air loading estimation are not given in this chapter and air loadings are assumed to be given. Methods to calculate the air loading to complete the equations and to enable it to be numerically calculated are given in the following chapters. In the actual aircraft, gravitational force also contributes, but this effect is neglected in this report. However, the gravitational force depends only on the mass distribution, so it could be easily included.

Since the blade is rigid in torsion, only lift and drag are considered in the blade equation of motions. The direction of lift and drag are determined by the direction of the inflow, including the rotor-induced velocity, which also depends upon the method of air loading estimation. To avoid additional assumptions, the blade air loading is given by the components in the rotational plane $p_{\theta n}$ (positive in the rotational direction) and out-of-rotational plane p_{zn} (positive forward), in the same directions as those used in defining the blade deformation. The forces acting in the radial direction are not considered since the blade is assumed to neither stretch nor shrink in that direction. Thus the virtual work in the equations of motion for the blade is given by

$$P_n^i = \int_0^R (p_{\theta n} V_i + p_{zn} W_i)\, dr \tag{27}$$

As for the case of the blade, wing loading is also given without specifying any aerodynamic theory. It is given in cruising direction f_z (positive forward) and upward direction f_x. The wing has a torsional degree of freedom and the torsional moment about the elastic axis is given by f_m (positive nose up). Then the virtual work G_i is

$$G_i = \int_0^L (f_x U_{Wi} + f_z W_{Wi} + m_e P_{Wi})\, dy \tag{28}$$

The virtual work on the wing by the blade air loading F_i is given using the wingtip positions $U_{Wi,tip}$ and $W_{Wi,tip}$, and its rotation $P_{Wi,tip}$.

$$F_i = \sum_{n=1}^{N} \int_0^R \left\{ \begin{pmatrix} U_{wi,tip} \\ 0 \\ W_{wi,tip} \end{pmatrix}^t (T) \begin{pmatrix} 0 \\ p_{\theta n} \\ p_{zn} \end{pmatrix} + \begin{pmatrix} W'_{Wi,tip} \\ P_{Wi,tip} \\ -U'_{Wi,tip} \end{pmatrix}^t (T) \left[\begin{pmatrix} r \\ v_n \\ h + w_n \end{pmatrix} \times \begin{pmatrix} 0 \\ p_{\theta n} \\ p_{zn} \end{pmatrix} \right] \right\} dr \tag{29}$$

The variable (T) is the transformation matrix from the rotating coordinate system fixed to the blade before deformation to the inertia coordinate system fixed to the aircraft and is given by

$$(T) = \begin{pmatrix} 1 & -\nu_r & \nu_p \\ \nu_r & 1 & -\nu_y \\ -\nu_p & \nu_y & 1 \end{pmatrix} \begin{pmatrix} \cos\psi_n & -\sin\psi_n & 0 \\ \sin\psi_n & \cos\psi_n & 0 \\ 0 & 0 & 1 \end{pmatrix} \tag{30}$$

Blade and wing deformation are expressed by the summation of natural modes for each degree of freedom.

$$w_n = \sum_{i=1}^{2} W_i(r) q_{ni}(t) \tag{31}$$

$$v_n = \sum_{i=1}^{2} V_i(r) q_{ni}(t) \tag{32}$$

$$u_w = \sum_{i=1}^{3} U_{Wi}(y) a_i(t) \tag{33}$$

$$w_w = \sum_{i=1}^{3} W_{Wi}(y) a_i(t) \tag{34}$$

$$p_w = \sum_{i=1}^{3} P_{Wi}(y) a_i(t) \tag{35}$$

$$r_x = \sum_{i=1}^{3} X_i a_i(t) \tag{36}$$

$$r_z = \sum_{i=1}^{3} Y_i a_i(t) \tag{37}$$

$$\nu_y = \sum_{i=1}^{3} N_{yi} a_i(t) \tag{38}$$

$$\nu_p = \sum_{i=1}^{3} N_{pi} a_i(t) \tag{39}$$

$$\nu_r = \sum_{i=1}^{3} N_{ri} a_i(t) \tag{40}$$

$$X_i = U_{Wi,tip} \tag{41}$$
$$Z_i = W_{Wi,tip} \tag{42}$$

$$N_{yi} = W'_{Wi,tip} \tag{43}$$
$$N_{pi} = P_{Wi,tip} \tag{44}$$
$$N_{ri} = -U'_{Wi,tip} \tag{45}$$

Even when a simple model is assumed, such as a fully articulated, nonelastic blade, the following formulation does not become simple because of the high inflow ratio. Each blade is controlled by cyclic and collective pitch; thus θ_n and q_{ni} are composed of three components

$$\theta_n = \theta_0(t) + \theta_s(t)\sin\psi_n + \theta_c(t)\cos\psi_n \tag{46}$$
$$q_{ni} = q_{i0}(t) + q_{is}(t)\sin\psi_n + q_{ic}(t)\cos\psi_n \tag{47}$$

Substituting those relations into the equations of motion, the following relations are obtained

Blade:

$$\begin{aligned}
&\ddot{q}_{i0} + \omega_i^2 q_{i0} \\
&\quad + (\ddot{q}_{is} - 2\Omega\dot{q}_{ic} - \Omega^2 q_{is} + \omega_i^2 q_{is})\sin\psi_n \\
&\quad + (\ddot{q}_{ic} + 2\Omega\dot{q}_{is} - \Omega^2 q_{ic} + \omega_i^2 q_{ic})\cos\psi_n \\
&\quad + \sum_{j=1}^{3}[Q^i_{1j}\ddot{a}_j + (Q^i_{2j}\ddot{a}_j + Q^i_{3j}\dot{a}_j)\sin\psi_n + (Q^i_{4j}\ddot{a}_j + Q^i_{5j}\dot{a}_j)\cos\psi_n] \\
&\quad = P^i_n.
\end{aligned} \tag{48}$$

$$Q^i_{1j} = -V_{1i}N_{rj} + W_{0i}\frac{Z_j}{R} \tag{49}$$
$$Q^i_{2j} = -\frac{V_{0i}}{R}(X_j + hN_{pj}) + W_{1i}N_{yj} \tag{50}$$
$$Q^i_{3j} = 2\Omega W_{1i}N_{pj} \tag{51}$$
$$Q^i_{4j} = -W_{1i}N_{pj} - \frac{h}{R}V_{0i}N_{yj} \tag{52}$$
$$Q^i_{5j} = 2\Omega W_{1i}N_{yj} \tag{53}$$

(where V_{0i}, V_{1i}, W_{0i}, and W_{1i} are given by equations (7) through (10))

Wing:

$$\ddot{a}_i + \omega_{wi}^2 a_i + I_B N \Omega \sum_{j=1}^{3} (N_{yi} N_{pj} - N_{pi} N_{yj}) \dot{a}_j$$

$$+ \sum_{n=1}^{N} \sum_{j=1}^{2} \Big\{ A_{1j}^i \ddot{q}_{j0} + \sin\psi_n \left[A_{1j}^i (\ddot{q}_{is} - 2\Omega \dot{q}_{ic} - \Omega^2 q_{is}) + A_{2j}^i \ddot{q}_{i0} + A_{4j}^i \dot{q}_{i0} + A_{6j}^i q_{i0} \right]$$

$$+ \cos\psi_n \left[A_{1j}^i (\ddot{q}_{ic} + 2\Omega \dot{q}_{is} - \Omega^2 q_{ic}) + A_{3j}^i \ddot{q}_{i0} + A_{5j}^i \dot{q}_{i0} + A_{7j}^i q_{i0} \right]$$

$$+ \frac{1 - \cos 2\psi_n}{2} \left[A_{2j}^i (\ddot{q}_{is} - 2\Omega \dot{q}_{ic} - \Omega^2 q_{is}) + A_{4j}^i (\dot{q}_{is} - \Omega q_{ic}) + A_{6j}^i q_{is} \right]$$

$$+ \frac{1 + \cos 2\psi_n}{2} \left[A_{3j}^i (\ddot{q}_{ic} + 2\Omega \dot{q}_{is} - \Omega^2 q_{ic}) + A_{5j}^i (\dot{q}_{ic} + \Omega q_{is}) + A_{7j}^i q_{ic} \right]$$

$$+ \frac{1}{2} \sin 2\psi_n \left[A_{2j}^i (\ddot{q}_{ic} + 2\Omega \dot{q}_{is} - \Omega^2 q_{ic}) + A_{3j}^i (\ddot{q}_{is} - 2\Omega \dot{q}_{ic} - \Omega^2 q_{is}) \right.$$

$$\left. + A_{4j}^i (\dot{q}_{ic} + \Omega q_{is}) + A_{5j}^i (\dot{q}_{is} - \Omega q_{ic}) + A_{6j}^i q_{ic} + A_{7j}^i q_{is} \right] \Big\}$$

$$= F_i + G_i \tag{54}$$

$$A_{1j}^i = V_{1j} N_{ri} + W_{0j} \frac{Z_i}{R} \tag{55}$$

$$A_{2j}^i = -\frac{V_{0j}}{R} (X_i + h N_{pi}) + W_{1j} N_{yi} \tag{56}$$

$$A_{3j}^i = -V_{0j} \frac{h}{R} N_{yi} - W_{1j} N_{pi} \tag{57}$$

$$A_{4j}^i = -2\Omega \frac{h}{R} V_{0j} N_{yi} \tag{58}$$

$$A_{5j}^i = -2\Omega \frac{V_{0j}}{R} (X_i + h N_{pi}) \tag{59}$$

$$A_{6j}^i = \Omega^2 \left[\frac{V_{0j}}{R} (X_i + h N_{pi}) + W_{1j} N_{yi} \right] \tag{60}$$

$$A_{7j}^i = \frac{1}{R} \Omega^2 (h V_{0j} N_{yi} - R W_{1j} N_{pi}) \tag{61}$$

When one compares the terms multiplying the constant (independent of ψ_n), $\sin\psi_n$ and $\cos\psi_n$ terms of equation (48) and the constant term of equation (54), the equations defining

q_{i0}, q_{is}, q_{ic}, and a_i are obtained

$$\ddot{q}_{i0} + \omega^2 q_0 + \sum_{j=1}^{3} Q^i_{1j} \ddot{a}_j = \left(P^i_n\right)_0 \tag{62}$$

$$\ddot{q}_{is} - 2\Omega \dot{q}_{ic} - (\Omega^2 - \omega_i^2) q_{is} + \sum_{j=1}^{3} (Q^i_{2j} \ddot{a}_j + Q^i_{3j} \dot{a}_j) = \left(P^i_n\right)_{\sin} \tag{63}$$

$$\ddot{q}_{ic} + 2\Omega \dot{q}_{is} - (\Omega^2 - \omega_i^2) q_{ic} + \sum_{j=1}^{3} (Q^i_{4j} \ddot{a}_j + Q^i_{5j} \dot{a}_j) = \left(P^i_n\right)_{\cos} \tag{64}$$

$$\begin{aligned}
&\ddot{a}_i + \omega^2_{wi} a_i + \sum_{j=1}^{3} I_B N \Omega (N_{yi} N_{pj} - N_{pi} N_{yj}) \dot{a}_j \\
&\qquad + \sum_{j=1}^{2} \Big[N A^i_{1j} \ddot{q}_{j0} + \frac{N A^i_{2j}}{2} \ddot{q}_{js} + \frac{N A^i_{3j}}{2} \ddot{q}_{jc} \\
&\qquad\quad + \frac{N}{2} \left(A^i_{4j} + 2\Omega A^i_{3j}\right) \dot{q}_{js} + \frac{N}{2} \left(A^i_{5j} - 2\Omega A^i_{2j}\right) \dot{q}_{jc} \\
&\qquad\quad + \frac{N}{2} \left(A^i_{6j} + \Omega A^i_{5j} - \Omega^2 A^i_{2j}\right) q_{js} \\
&\qquad\quad + \frac{N}{2} \left(A^i_{7j} - \Omega A^i_{4j} - \Omega^2 A^i_{3j}\right) q_{jc} \Big] \\
&\qquad = (F_i + G_i)_0
\end{aligned} \tag{65}$$

where subscripts $(\,)_0$, $(\,)_{\sin}$, and $(\,)_{\cos}$ indicate constant (independent of azimuth angle) terms, $\sin\psi_n$, and $\cos\psi_n$ terms, respectively, which are considered next. The number of blades N is assumed to be odd and greater than two in these equations, but the calculations for an even-bladed rotor can be done in a similar manner.

The virtual work terms on the right hand side of equations of motion (62) through (65), need to be determined next. The terms should be in a linear form to apply the harmonic method. The deflection itself, rather than the deflection from the equilibrium state, is used in the linearization. Thus, the coefficients of generalized coordinates (i.e., coefficients for the first order in Taylor expansion) are different from those at a deflected equilibium point. However, the equilibrium value is not correct under the simplifications involved in

the air loading calculations, especially using a simple aerodynamic theory. This approach was chosen to avoid additional assumptions and to make the following calculations simple. Figure 5 gives schematic views of the air loading geometry on the blade and the wing. The blade aerodynamic force is calculated using quasi-steady theory. The Prandtl-Glauert rule is applied to correct for compressibility effects. The blade lift and drag per unit span, l and d, respectively, and the in-plane and out-of-plane aerodynamic forces $p_{\theta n}$ and p_{zn} are written as

$$p_{\theta n} = -l\sin\phi - d\cos\phi \tag{66}$$

$$p_{zn} = l\cos\phi - d\sin\phi \tag{67}$$

$$l = \frac{1}{2\sqrt{1-M^2}}\rho V_R^2\, c\, C_{l\alpha}\alpha \tag{68}$$

$$d = \frac{1}{2}\rho V_R^2 c C_d \tag{69}$$

$$V_R = \sqrt{V^2 + (r\Omega)^2} \tag{70}$$

$$\phi = \tan^{-1}\left(\frac{V}{r\Omega}\right) \tag{71}$$

The blade-angle-of-attack equation is

$$\alpha = \theta - \phi + \frac{1}{V_R}(v_{in}\sin\phi - v_{out}\cos\phi) \tag{72}$$

$$v_{in} = \dot{v}_j + r\dot{\nu}_r + (-\dot{r}_x - h\dot{\nu}_p + V\nu_p)\sin\psi_n + (-h\dot{\nu}_y + V\nu_y)\cos\psi_n \tag{73}$$

$$v_{out} = \dot{w}_j + \dot{r}_z + r\dot{\nu}_y\sin\psi_n - r\dot{\nu}_p\cos\psi_n \tag{74}$$

where v_{in} and v_{out} are the air-velocity components relative to the blade caused by wing deformation, and ϕ is the inflow angle. The induced velocity is neglected, since it is small in comparison with cruising velocity, and stability not static deflections is the major concern of this study. When v_{in} and v_{out} are written in terms of natural modes and Fourier-type generalized coordinates, the following relations are obtained

$$\begin{aligned} &v_{in}\sin\phi - v_{out}\cos\phi \\ &\quad = \sum_{j=1}^{2} S_{B1j}\dot{q}_{j0} + \sum_{j=1}^{3} S_{W1j}\dot{a}_j \\ &\qquad + \sin\psi_n\left(\sum_{j=1}^{2} S_{B2j}\dot{q}_{js} + \sum_{j=1}^{2} S_{B3j}q_{jc} + \sum_{j=1}^{3} S_{W2j}\dot{a}_j + \sum_{j=1}^{3} S_{W3j}a_j\right) \\ &\qquad + \cos\psi_n\left(\sum_{j=1}^{2} S_{B4j}\dot{q}_{jc} + \sum_{j=1}^{2} S_{B5j}q_{js} + \sum_{j=1}^{3} S_{W4j}\dot{a}_j + \sum_{j=1}^{3} S_{W4j}a_j\right) \end{aligned} \tag{75}$$

$$S_{B1j} = V_j \sin\phi - W_j \cos\phi \tag{76}$$
$$S_{B2j} = S_{B1j} \tag{77}$$
$$S_{B3j} = -\Omega S_{B1j} \tag{78}$$
$$S_{B4j} = S_{B1j} \tag{79}$$
$$S_{B5j} = \Omega S_{b1j} \tag{80}$$
$$S_{W1j} = rN_{rj} \sin\phi - Z_j \cos\phi \tag{81}$$
$$S_{W2j} = -(X_j + hN_{pj}) \sin\phi - rN_{yj} \cos\phi \tag{82}$$
$$S_{W3j} = VN_{pj} \sin\phi \tag{83}$$
$$S_{W4j} = -hN_{yj} \sin\phi + rN_{pj} \cos\phi \tag{84}$$
$$S_{W5j} = VN_{yj} \sin\phi \tag{85}$$

The relations (66) through (85) give blade and wing air loading in terms of the generalized coordinates. Substituting equations (66) and (67) into (27), the virtual work on the blade caused by the blade air loading is given as follows:

$$\begin{aligned} P_n^i =& I_{B0}^i + \sum_{j=1}^{2} I_{B1j}^i \dot{q}_{j0} + \sum_{j=1}^{3} I_{W1j}^i \dot{a}_j \\ &+ \left(\sum_{j=1}^{2} I_{B2j}^i \dot{q}_{js} + \sum_{j=1}^{2} I_{B3j}^i q_{jc} + \sum_{j=1}^{3} I_{W2j}^i \dot{a}_j - \sum_{j=1}^{3} I_{W3J}^i a_j + I_S^i \theta_s \right) \sin\psi_n \\ &+ \left(\sum_{j=1}^{2} I_{B4j}^i \dot{q}_{jc} + \sum_{j=1}^{2} I_{B5j}^i q_{js} + \sum_{j=1}^{3} I_{W4j}^i \dot{a}_j - \sum_{j=1}^{3} I_{W5J}^i a_j + I_C^i \theta_c \right) \cos\psi_n \end{aligned} \tag{86}$$

$$\begin{aligned} I_{B0}^i = & -\frac{1}{2}\rho C_{l\alpha} \int_0^R \frac{1}{\sqrt{1-M^2}} c V_R^2 (\theta - \phi)(V_i \sin\phi - W_i \cos\phi)\, dr \\ & - \frac{1}{2}\rho \int_0^R c C_d V_R^2 (V_i \cos\phi + W_i \sin\phi)\, dr \end{aligned} \tag{87}$$

$$I_{B1j}^i = -\frac{1}{2}\rho C_{l\alpha} \int_0^R \frac{1}{\sqrt{1-M^2}} V_R c S_{B1j} (V_i \sin\phi - W_i \cos\phi)\, dr \tag{88}$$

$$I_{B2j}^i = -\frac{1}{2}\rho C_{l\alpha} \int_0^R \frac{1}{\sqrt{1-M^2}} V_R c S_{B2j} (V_i \sin\phi - W_i \cos\phi)\, dr \tag{89}$$

$$I_{B3j}^i = -\frac{1}{2}\rho C_{l\alpha} \int_0^R \frac{1}{\sqrt{1-M^2}} V_R c S_{B3j} (V_i \sin\phi - W_i \cos\phi)\, dr \tag{90}$$

$$I^i_{B4j} = -\frac{1}{2}\rho\, C_{l\alpha} \int_0^R \frac{1}{\sqrt{1-M^2}} V_R c S_{B4j} (V_i \sin\phi - W_i \cos\phi)\, dr \tag{91}$$

$$I^i_{B5j} = -\frac{1}{2}\rho\, C_{l\alpha} \int_0^R \frac{1}{\sqrt{1-M^2}} V_R c S_{B5j} (V_i \sin\phi - W_i \cos\phi)\, dr \tag{92}$$

$$I^i_{W1j} = -\frac{1}{2}\rho\, C_{l\alpha} \int_0^R \frac{1}{\sqrt{1-M^2}} V_R c S_{W1j} (V_i \sin\phi - W_i \cos\phi)\, dr \tag{93}$$

$$I^i_{W2j} = -\frac{1}{2}\rho\, C_{l\alpha} \int_0^R \frac{1}{\sqrt{1-M^2}} V_R c S_{W2j} (V_i \sin\phi - W_i \cos\phi)\, dr \tag{94}$$

$$I^i_{W3j} = -\frac{1}{2}\rho\, C_{l\alpha} \int_0^R \frac{1}{\sqrt{1-M^2}} V_R c S_{W3j} (V_i \sin\phi - W_i \cos\phi)\, dr \tag{95}$$

$$I^i_{W4j} = -\frac{1}{2}\rho\, C_{l\alpha} \int_0^R \frac{1}{\sqrt{1-M^2}} V_R c S_{W4j} (V_i \sin\phi - W_i \cos\phi)\, dr \tag{96}$$

$$I^i_{W5j} = -\frac{1}{2}\rho\, C_{l\alpha} \int_0^R \frac{1}{\sqrt{1-M^2}} V_R c S_{W5j} (V_i \sin\phi - W_i \cos\phi)\, dr \tag{97}$$

$$I^i_C = -\frac{1}{2}\rho\, C_{l\alpha} \int_0^R \frac{1}{2} V_R^2 (V_i \sin\phi - W_i \cos\phi)\, dr \tag{98}$$

$$I^i_S = I^i_C \tag{99}$$

The virtual work on the wing done by the rotor-blade air loading, given by equation (29), is

$$F_i = \sum_{n=1}^{N} \int_0^R \left\{ \begin{pmatrix} U_{Wi,tip} \\ 0 \\ W_{Wi,tip} \end{pmatrix}^t (T) \begin{pmatrix} 0 \\ p_{\theta n} \\ p_{zn} \end{pmatrix} + \begin{pmatrix} W'_{Wi,tip} \\ P_{Wi,tip} \\ -U'_{Wi,tip} \end{pmatrix}^t (T) \left[\begin{pmatrix} r \\ v_n \\ h + w_n \end{pmatrix} \times \begin{pmatrix} 0 \\ p_{\theta n} \\ p_{zn} \end{pmatrix} \right] \right\} dr$$

$$= \sum_{j=1}^{3} K^i_{W1j} \dot{a}_j + \sum_{j=1}^{3} K^i_{W2j} a_j + \sum_{j=1}^{2} K^i_{B1j} \dot{q}_{j0} + \sum_{j=1}^{2} K^i_{B2j} \dot{q}_{js} + \sum_{j=1}^{2} K^i_{B1j} \dot{q}_{j0} + \sum_{j=1}^{2} K^i_{B2j} \dot{q}_{js}$$

$$+\sum_{j=1}^{2} K^i_{B3j}\dot{q}_{jc} + \sum_{j=1}^{2} K^i_{B4j}q_{j0}$$
$$+\sum_{j=1}^{2} K^i_{B5j}q_{js} + \sum_{j=1}^{2} K^i_{B6j}q_{jc}$$
$$+ K^i_S\theta_s + K^i_C\theta_c + K^i_0 \tag{100}$$

Details of K^i_{Wkj}, K^i_{Bkj}, K^i_S, K^i_C and K^i_0 are given in appendix A.

The wing aerodynamics are more complicated because of the pitching motion. When some aerodynamics theories are referred to as quasi-steady, the reference often means the usage of wing velocity relative to air, neglecting the effect of shed vortices. When pitching motion is introduced, wing velocity relative to the air varies along the chord. Aerodynamic force becomes dependent upon the point used to represent the wing motion. It is not appropriate to take the elastic axis as a representative point, since the air forces are not directly related to blade elasticity. In steady or unsteady aerodynamics (such as lifting-surface theory or Theodorsen's theory) the three-quarter chord line is an important point to represent the boundary condition. In this formulation the boundary condition for the angle of attack is at the three-quarter chord line, and the effect of shed vortices is disregarded. The wing aerodynamic force is given by lift l_w, drag d_w and pitching moment around the elastic axis m_e

$$\begin{aligned} l_w &= \frac{1}{2}\rho V^2 c_w C_{l\alpha}\left[\theta_w + p_w - \frac{v_d + \dot{u}_w - (0.75 - a_e)c_w\dot{p}_w}{V + \dot{w}_w}\right] \\ &\approx \frac{1}{2}\rho V^2 c_w C_{l\alpha}\left[\theta_w + p_w - \frac{v_d + \dot{u}_w - (0.75 - a_e)c_w\dot{p}_w}{V} + \frac{v_d\dot{w}_w}{V^2}\right] \end{aligned} \tag{101}$$

$$m_e = \frac{1}{2}\rho V^2 c_w C_m + l(a_e - 0.25)c_w \tag{102}$$

where C_m is the pitching-moment coefficient about the aerodynamic center (which is assumed to fall on the one-quarter chord line), and $a_e c_w$ is the distance between the leading edge and the wing elastic axis. Downwash caused by the wing itself is denoted by v_d and is given using the geometrical angle of attack θ_w and the wing-aspect ratio A_W

$$v_d = \frac{2 - A_W + \sqrt{4 + A_W^2}}{2 + \sqrt{4 + A_W^2}} V\theta_w \tag{103}$$

The inclination of lift is expressed as $\phi_w = v_d/V$. When this inclination of lift is assumed unchanged to be, the aerodynamic force on the wing is given in the X and Y directions

as $(l_w \cos\phi_w - 0.5\rho V^2 c_w C_d \sin\phi_w,\ -l_w \sin\phi_w + 0.5\rho V^2 c_w C_d \cos\phi_w)$. The virtual work on the wing done by the wing aerodynamic forces is given by

$$G_i = \int_0^L \begin{pmatrix} l_w \cos\phi_w - 0.5\rho V^2 c_w C_d \sin\phi_w \\ -l_w \sin\phi_w + 0.5\rho V^2 c_w C_d \cos\phi_w \\ m_e \end{pmatrix}^t \begin{pmatrix} U_{Wi} \\ W_{Wi} \\ P_{Wi} \end{pmatrix} dy$$

$$= G^i_{W1} + \sum_{j=1}^{3} G^i_{W2j}\, a_j + \sum_{j=1}^{3} G^i_{W3j}\, \dot{a}_j \tag{104}$$

$$G^i_{W1} = \int_0^L \frac{1}{2}\rho V c_w C_{l\alpha}(V\theta_w - v_d)\cdot$$

$$[U_{Wi}\cos\phi_w - W_{Wi}\sin\phi_w + (a_e - 0.25)c_w P_{Wi}]\, dy$$

$$- \int_0^L \frac{1}{2}\rho V^2 c_w C_d (U_{Wi}\sin\phi_w + W_{Wi}\cos\phi_w)\, dy$$

$$+ \int_0^L \frac{1}{2}\rho V^2 c_w^2 C_m P_{Wi}\, dr \tag{105}$$

$$G^i_{W2j} = \int_0^L \frac{1}{2}\rho c_w C_{l\alpha} V^2 P_{Wj}\cdot$$

$$[U_{Wi}\cos\phi_w - W_{Wi}\sin\phi_w + (a_e - 0.25)c_w P_{Wi}]\, dy \tag{106}$$

$$G_{W3j} = \int_0^L \frac{1}{2}\rho c_w C_{l\alpha}[-V U_{Wj} + (0.75 - a_e)V c_w P_{Wj} - v_d W_{Wj}]\cdot$$

$$[U_{Wi}\cos\phi_w - W_{Wi}\sin\phi_w + (a_e - 0.25)c_w P_{Wi}]\, dr \tag{107}$$

After the virtual work is written in terms of generalized coordinates, and when one compares the terms multiplying the constant (independent of azimuth angle ψ_n), $\sin\psi_n$ and $\cos\psi_n$ terms, the following equations are obtained for the blade equation of motion

$$\ddot{q}_{i0} + \omega_i^2 q_{i0} + \sum_{j=1}^{3} Q^i_{1j}\, \ddot{a}_j - \sum_{j=1}^{2} I^i_{B1j}\dot{q}_{j0} - \sum_{j=1}^{3} I^i_{W1j}\dot{a}_j = I^i_{B0} \tag{108}$$

$$\ddot{q}_{is} + (\omega_i^2 - \Omega^2)q_{is} - 2\Omega\,\dot{q}_{ic} + \sum_{j=1}^{3} Q^i_{2j}\ddot{a}_j + \sum_{j=1}^{3} Q^i_{3j}\dot{a}_j$$

$$
\begin{aligned}
&- \sum_{j=1}^{2} I^i_{B2j} \dot{q}_{js} - \sum_{j=1}^{2} I^i_{B3j} q_{jc} \\
&- \sum_{j=1}^{3} I^i_{W2j} \dot{a}_j - \sum_{j=1}^{3} I^i_{W3j} a_j = I^i_S \theta_s
\end{aligned} \tag{109}
$$

$$
\begin{aligned}
&\ddot{q}_{ic} + (\omega_i^2 - \Omega^2) q_{ic} + 2\Omega \dot{q}_{is} + \sum_{j=1}^{3} Q^i_{4j} \ddot{a}_j + \sum_{j=1}^{3} Q^i_{5j} \dot{a}_j \\
&- \sum_{j=1}^{2} I^i_{B4j} \dot{q}_{jc} - \sum_{j=1}^{2} I^i_{B5j} q_{js} \\
&- \sum_{j=1}^{3} I^i_{W4j} \dot{a}_j - \sum_{j=1}^{3} I^i_{W5j} a_j = I^i_C \theta_c
\end{aligned} \tag{110}
$$

In the same way, by substituting equations (100) and (104) into equation (54), the following equation is obtained from the constant term of the wing equation of motion:

$$
\begin{aligned}
&\ddot{a}_i + \omega^2_{wi} a_i + \sum_{j=1}^{3} \left[I_B N \Omega (N_{yi} N_{pj} - N_{pi} N_{yj}) - G^i_{W3j} - K^i_{W1j} \right] \dot{a}_j \\
&- \sum_{j=1}^{3} (G^i_{W2j} + K^i_{W2j}) a_j \\
&+ \sum_{j=1}^{2} N A^i_{1j} \ddot{q}_{j0} - \sum_{j=1}^{2} K^i_{B1j} \dot{q}_{j0} + \sum_{j=1}^{2} K^i_{B4j} q_{j0} \\
&+ \sum_{j=1}^{2} \frac{N}{2} A^i_{2j} \ddot{q}_{js} + \sum_{j=1}^{2} \left(\frac{N}{2} A^i_{4j} + N\Omega A^i_{3j} - K^i_{B2j} \right) \dot{q}_{js} \\
&+ \sum_{j=1}^{2} \left(\frac{N}{2} A^i_{6j} + \frac{N}{2} \Omega A^i_{5j} - \frac{N}{2} \Omega^2 A^i_{2j} - K^i_{B5j} \right) q_{js} \\
&+ \sum_{j=1}^{2} \frac{N}{2} A^i_{3j} \ddot{q}_{jc} + \sum_{j=1}^{2} \left(\frac{N}{2} A^i_{5j} - N\Omega A^i_{2j} - K^i_{B4j} \right) \dot{q}_{jc} \\
&+ \sum_{j=1}^{2} \left(\frac{N}{2} A^i_{7j} - \frac{N}{2} \Omega A^i_{4j} - \frac{N}{2} \Omega^2 A^i_{3j} - K^i_{B6j} \right) q_{jc}
\end{aligned}
$$

$$= K_S^i \theta_s + K_C^i \theta_c + K_0^i \tag{111}$$

Final equations of motion for the generalized coordinates in equations (108) through (110) are written in the following form:

$$\mathbf{E}^2 \ddot{\mathbf{X}} + \mathbf{E}^1 \dot{\mathbf{X}} + \mathbf{E}^0 \mathbf{X} = \mathbf{D} \begin{pmatrix} \theta_0 & \theta_s & \theta_c \end{pmatrix}^t \tag{112}$$

$$\mathbf{E}^n = \begin{pmatrix} E^n_{1,1} & E^n_{1,2} & \cdots & E^n_{1,9} \\ E^n_{2,1} & E^n_{2,2} & \cdots & E^n_{2,9} \\ \vdots & \vdots & \ddots & \vdots \\ E^n_{9,1} & E^n_{9,2} & \cdots & E^n_{9,9} \end{pmatrix} \tag{113}$$

$$\mathbf{D} = \begin{pmatrix} D_{1,1} & D_{1,2} & D_{1,3} \\ D_{2,1} & D_{2,2} & D_{2,3} \\ \vdots & \vdots & \vdots \\ D_{9,1} & D_{9,2} & D_{9,3} \end{pmatrix} \tag{114}$$

$$\mathbf{X} = \begin{pmatrix} q_{10}, & q_{1s}, & q_{1c}, & q_{20}, & q_{2s}, & q_{2c}, & a_1, & a_2, & a_3 \end{pmatrix}^t \tag{115}$$

Details of the elements E^n_{ij} and D_{ij} are given in appendix B.

DESIGN OF CONTROL SYSTEM

One approach to suppress coupled wing/rotor self-exited oscillation is active pitch control of the rotor blade (references 8-11). The tilt-rotor aircraft has other control surfaces, such as a flaperon. However, only the pitch control using a conventional swashplate is considered here. The control system is a simple feedback system which uses wing-deflection feedback. The possibility of flutter control is investigated using a harmonic balance method. For simplicity, air loading is calculated here using a two-dimensional strip theory for both the wing and the rotor blade. In the following analysis, the gravitational force is neglected. When blade pitch control is introduced, the natural frequencies and corresponding mode shape of the system vary as a function of time. This change is not considered and the natural frequency and mode shape are assumed to be valid for a specific flight condition.

This formulation uses generalized coordinates. What actually can be measured in flight is not a generalized coordinate but the actual deflection or its derivative, which is given by an infinite series of generalized coordinates. There are two choices in introducing a feedback control system: one uses a generalized coordinate as input for the control system, and the other uses an actual deflection or a rate of deflection. The latter is chosen here.

The wing deflection speed and the acceleration at the wingtip are used for the feedback input. Cyclic pitch control is given by

$$\begin{aligned}\theta_s = & K_{usd}\dot{u}_{w,tip} + K_{usdd}\ddot{u}_{w,tip} \\ & + K_{wsd}\dot{w}_{w,tip} + K_{wsdd}\ddot{w}_{w,tip} \\ & + K_{psd}\dot{p}_{w,tip} + K_{psdd}\ddot{p}_{w,tip}\end{aligned} \tag{116}$$

$$\begin{aligned}\theta_c = & K_{ucd}\dot{u}_{w,tip} + K_{ucdd}\ddot{u}_{w,tip} \\ & + K_{wcd}\dot{w}_{w,tip} + K_{wcdd}\ddot{w}_{w,tip} \\ & + K_{pcd}\dot{p}_{w,tip} + K_{pcdd}\ddot{p}_{w,tip}\end{aligned} \tag{117}$$

Using this control law, the final equation is modified to

$$\mathbf{E}^{2c}\ddot{\mathbf{X}} + \mathbf{E}^{1c}\dot{\mathbf{X}} + \mathbf{E}^{0c}\mathbf{X} = \mathbf{D}\,(\theta_0 \quad 0 \quad 0)^t \tag{118}$$

$$\begin{aligned}\mathbf{E}^{2c} = \mathbf{E}^2 & - (K_{vsdd}\mathbf{B}^s + K_{vcdd}\mathbf{B}^c)\,\mathbf{V} \\ & - (K_{wsdd}\mathbf{B}^s + K_{wcdd}\mathbf{B}^c)\,\mathbf{W} \\ & - (K_{psdd}\mathbf{B}^s + K_{pcdd}\mathbf{B}^c)\,\mathbf{P}\end{aligned} \tag{119}$$

$$\begin{aligned}\mathbf{E}^{1c} = \mathbf{E}^1 & - (K_{vsd}\mathbf{B}^s + K_{vcd}\mathbf{B}^c)\,\mathbf{V} \\ & - (K_{wsd}\mathbf{B}^s + K_{wcd}\mathbf{B}^c)\,\mathbf{W} \\ & - (K_{psd}\mathbf{B}^s + K_{pcd}\mathbf{B}^c)\,\mathbf{P}\end{aligned} \tag{120}$$

$$\mathbf{E}^{0c} = \quad \mathbf{E}^0 \tag{121}$$

$$\mathbf{B}^s = \begin{pmatrix} I_S^1 & I_S^1 & I_S^1 \\ 0 & 0 & 0 \\ 0 & 0 & 0 \\ I_S^2 & I_S^2 & I_S^2 \\ 0 & 0 & 0 \\ 0 & 0 & 0 \\ K_S^1 & K_S^1 & K_S^1 \\ K_S^2 & K_S^2 & K_S^2 \\ K_S^3 & K_S^3 & K_S^3 \end{pmatrix} \tag{122}$$

$$\mathbf{B}^c = \begin{pmatrix} I_C^1 & I_C^1 & I_C^1 \\ 0 & 0 & 0 \\ 0 & 0 & 0 \\ I_C^2 & I_C^2 & I_C^2 \\ 0 & 0 & 0 \\ 0 & 0 & 0 \\ K_C^1 & K_C^1 & K_C^1 \\ K_C^2 & K_C^2 & K_C^2 \\ K_C^3 & K_C^3 & K_C^3 \end{pmatrix} \tag{123}$$

$$\mathbf{V} = \begin{pmatrix} 0 & 0 & 0 & 0 & 0 & 0 & V_{W1,tip} & V_{W1,tip} & V_{W1,tip} \\ 0 & 0 & 0 & 0 & 0 & 0 & V_{W2,tip} & V_{W2,tip} & V_{W2,tip} \\ 0 & 0 & 0 & 0 & 0 & 0 & V_{W3,tip} & V_{W3,tip} & V_{W3,tip} \end{pmatrix} \tag{124}$$

$$\mathbf{W} = \begin{pmatrix} 0 & 0 & 0 & 0 & 0 & 0 & W_{W1,tip} & W_{W1,tip} & W_{W1,tip} \\ 0 & 0 & 0 & 0 & 0 & 0 & W_{W2,tip} & W_{W2,tip} & W_{W2,tip} \\ 0 & 0 & 0 & 0 & 0 & 0 & W_{W3,tip} & W_{W3,tip} & W_{W3,tip} \end{pmatrix} \tag{125}$$

$$\mathbf{P} = \begin{pmatrix} 0 & 0 & 0 & 0 & 0 & 0 & P_{W1,tip} & P_{W1,tip} & P_{W1,tip} \\ 0 & 0 & 0 & 0 & 0 & 0 & P_{W2,tip} & P_{W2,tip} & P_{W2,tip} \\ 0 & 0 & 0 & 0 & 0 & 0 & P_{W3,tip} & P_{W3,tip} & P_{W3,tip} \end{pmatrix} \tag{126}$$

The stability of the system, whose motion is given by equation (118), is defined by the eigenvalues of the following matrix $\mathbf{S}$.

$$\mathbf{S} = \begin{pmatrix} -\mathbf{E}^{2cI}\mathbf{E}^{1c} & -\mathbf{E}^{2cI}\mathbf{E}^{0c} \\ \mathbf{I}_9 & \mathbf{0}_9 \end{pmatrix} \tag{127}$$

where $\mathbf{E}^{2cI}$, $\mathbf{I}_9$, and $\mathbf{0}_9$ indicate the inverse matrix of $\mathbf{E}^{2c}$, a unit matrix of order nine, and a zero square matrix of order nine, respectively.

TIMEWISE CALCULATION

To make a transient numerical calculation for the tilt-rotor's coupled-wing and blade deflections, and to evaluate the control law given in the previous section, a method is

given for independent timewise calculations. Determination of the control law is based on a rather simple theory. A more sophisticated aerodynamics theory and two or more natural oscillatory modes for each degree of freedom are employed in the transient analysis.

Most of the aeroelastic studies conducted previously have been using quasi-steady and strip theory. In this study the aerodynamic force is calculated on the basis of an unsteady theory. The calculation is based on Weissinger's concept through a vortex lattice method for the wing and on a local circulation method for the rotor blade (both with modifications to take the shed-vortex effect into account). Unsteady aerodynamics is a very complex problem even for a fixed wing with infinite aspect ratio. To get a precise solution requires large amounts of computer time. As for this study an efficient timewise calculation of tilt-rotor motion was desired, the following formulation aims at a rapid calculation rather than an exact solution. Arbitrary wing or rotor-blade motion is treated as a superposition of harmonic motions for a short interval to make the calculation simple. Then, for each harmonic motion, wing theory in harmonic motion is applied.

Wing lift l_w and pitching moment m_e consist of three components: steady components l_s and m_s, harmonic components l_k and m_k, and virtual-mass components l_v and m_v:

$$l_w = l_s + \sum_k l_k + l_v \tag{128}$$

$$m_e = m_s + \sum_k m_k + m_v. \tag{129}$$

As the shed vortex distribution depends upon the history of the wing motion the wing deformation and its derivatives are expressed as a series of harmonic components, using their previous values:

$$u_w = u_{w0} + \sum_k \bar{u}_{wk} e^{i\omega_k t} \tag{130}$$

$$\dot{u}_w = \dot{u}_{w0} + \sum_k \bar{\dot{u}}_{wk} e^{i\omega_k t} \tag{131}$$

$$w_w = w_{w0} + \sum_k \bar{w}_{wk} e^{i\omega_k t} \tag{132}$$

$$\dot{w}_w = \dot{w}_{w0} + \sum_k \bar{\dot{w}}_{wk} e^{i\omega_k t} \tag{133}$$

$$p_w = p_{w0} + \sum_k \bar{p}_{wk} e^{i\omega_k t} \tag{134}$$

$$\dot{p}_w = \dot{p}_{w0} + \sum_k \bar{\dot{p}}_{wk} e^{i\omega_k t} \tag{135}$$

where variables with a bar represent complex numbers.

The boundary condition at the position bc_w from the leading edge is

$$\dot{u} = -\dot{u}_w + \dot{p}_w(b - a_w)c_w + (V + \dot{w}_w)(\theta_w + p_w) \tag{136}$$

When the deflection and its time derivative are assumed to be small, the equation is linearized as

$$\dot{u} = -\dot{u}_w + \dot{p}_w(b - a_w)c_w + V(\theta_w + p_w) + \dot{w}_w\theta_w \tag{137}$$

The steady lift component is calculated through Weissinger's concept. At the three-quarter chord line, the downwash velocity is given by

$$\dot{u}_{0.75} = -\dot{u}_w + \dot{p}_w(0.75 - a_w)c_w + V(\theta_w + p_w) + \dot{w}_w\theta_w \tag{138}$$

Since this value is dependent upon time, it is not directly used in the boundary condition for the air loading calculation. The steady component of the air loading is calculated using the constant term of this air velocity as the boundary condition in a vortex lattice method

$$\dot{u}_c = -\dot{u}_{w0} + \dot{p}_{w0}(0.75 - a_w)c_w + V(\theta_w + p_{w0}) + \dot{w}_{w0}\theta_w \tag{139}$$

Steady pitching moment around the elastic axis m_s is attributed to wing airfoil shape and is given using the pitching-moment coefficient for a steady airfoil

$$m_s = \frac{1}{2}\rho V^2 c_w^2 C_m - l_s(0.25 - a_w)c_w \tag{140}$$

The steady lift given in this way is accurate in the sense that the shed vortex effect does not exist and that the trailing vortex effect is included.

The unsteady components (harmonic components and virtual mass components) are more difficult to estimate. Even under the assumptions just given (sinusoidally oscillating air loading), there is not an easy and versatile calculation method which properly includes shed vortex and trailing vortex effects. As stated previously, this study aims at the efficient timewise calculation of tilt-rotor motion. Air loading l_k, caused by the kth harmonic motion is calculated using a two-dimensional theory. Aspect ratio and spanwise location are taken into account by multiplying l_k by a factor η:

$$l_k = \eta C_{l\alpha}\rho V\frac{c_w}{2}C\left(\frac{\omega_k c_w}{2V}\right)(-\bar{\dot{u}}_{wk} + V\bar{p}_{wk} + (0.75 - a_w)c_w\bar{\dot{p}}_{wk} + \bar{\dot{w}}_{wk}\theta_w) \tag{141}$$

$$m_k = -l_k(0.25 - a_w)c_w \tag{142}$$

where $C\left(\omega_k c_w/2V\right)$ is the Theodorsen function, and the factor η is given by

$$\eta = \eta_1 \eta_2 \tag{143}$$

$$\eta_1 = \frac{A_w}{2 + \sqrt{4 + A_w^2}} \tag{144}$$

$$\eta_2 = \frac{4}{\pi}\sqrt{1 - \left(\frac{y}{L}\right)^2} \tag{145}$$

$$A_w = \frac{(2L)^2}{S_w} \tag{146}$$

The variable η_1 is the correction for finite aspect ratio A_w, and η_2 is calculated under an assumption that this air loading is distributed elliptically along the span. The air loading caused by the virtual mass motion is also given by two-dimensional theory with the same correction:

$$l_v = \eta(l_2 + l_3) \tag{147}$$

$$m_v = \eta(m_2 + m_3 + m_4) \tag{148}$$

$$l_2 = \rho\pi\left(\frac{c_w}{2}\right)^2 \left(-\ddot{u}_w + (0.5 - a_w)c_w\ddot{p}_w\right) \tag{149}$$

$$l_3 = \rho\pi\left(\frac{c_w}{2}\right)^2 V\dot{p}_w \tag{150}$$

$$m_2 = -l_2\left(0.25 - a_w\right)c_w \tag{151}$$

$$m_3 = -l_3(0.75 - a_w)c_w \tag{152}$$

$$m_4 = -\frac{1}{8}\rho\pi\left(\frac{c_w}{2}\right)^4 \ddot{p}_w. \tag{153}$$

Drag is calculated using a drag coefficient

$$d = \frac{1}{2}\rho V^2 c_w C_d \tag{154}$$

These equations give the lift, drag, and pitching moment, but not the directions of lift and drag. In the case of lifting-surface theory, the most accurate expression of lift and induced drag is the sum of integration of lift along the chord line and leading-edge suction. Because of the simplification, where the chordwise distribution of bound vortex is not taken into account, this expression is not available in the present method. The most

suitable form for this simple case is that the lift is inclined backward by an amount, equal to the angle between the free flow and the lifting line (the same expression as that in simple lifting-line theory). It is sometimes discussed in the term of induced drag, and it is known that the estimation of induced drag is difficult even in a complete lifting surface theory. The lift and drag values are converted into air-load components in x and z direction (l_x and l_z)

$$l_x = l\cos\phi_w - d\sin\phi_w \tag{155}$$

$$l_z = -l\sin\phi_w - d\cos\phi_w \tag{156}$$

The calculation of lift-inclination angle ϕ_w is given in appendix C with the formulation of a vortex lattice method.

The blade air loading calculation is similar to that of the wing, except that it is based on the local circulation method instead of a vortex lattice method and that it lacks the torsional degree of freedom. The details of the local circulation method are described in refernces 2 and 3. Here the method used in the unsteady modification is stated. Among two dimensional theories of harmonic air loading, Theodorsen's and Sears' theories are widely used. Blade deflection in two directions, in plane and out of plane, is treated just like the wing case. Apart from the deflection, the blade encounters the induced velocity field made by the returning vortex; hence the local circulation method is better explained by the Sears' theory. However, as stated previously, because this model does not have a pitching degree of freedom, and because the Sears function can be approximated by the Theodorsen function when reduced frequency is small, this remaining induced velocity is included in the boundary condition on the blade element. Harmonic air loading is calculated using Theodorsen's theory in this study (reference 12). The air loading caused by virtual-mass effects is added afterward, because the relation of induced velocity and circulation is given by the quasi-steady assumption; thus, it does not contain virtual mass or acceleration terms at all. In this calculation, variation of pylon direction is assumed to be small, so rotor-blade air loading is calculated using the theory for axial flight.

The components of blade lift are steady lift, harmonic lift, and virtual mass lift

$$l_b = l_s + \sum_k l_k + l_v \tag{157}$$

The blade motion relative to the air is composed of cruising velocity, rotating velocity, induced velocity, and blade- and wing-deformation velocity (figure 6). These velocities give the geometrical angle of attack at the elastic axis as

$$\alpha_G = \theta - \phi - \frac{\dot{v}_p + u_s\cos\phi}{U} \tag{158}$$

$$\phi = \tan^{-1}\frac{V}{r\Omega} \tag{159}$$

$$U = \sqrt{(r\Omega)^2 + V^2} \tag{160}$$

When $\dot{v}_p$ is written in terms of in-plane and out-of-plane deformations equations (158) becomes

$$\alpha_G = \theta - \phi - \frac{u_t}{U} \tag{161}$$

$$\begin{aligned} u_t = {} & (u_s - \dot{w} - \dot{w}_w - r\dot{\nu}_y \sin\psi_n + r\dot{\nu}_p \cos\psi_n)\cos\phi \\ & + [\dot{v} + r\dot{\nu}_r + (-\dot{u}_w - h\dot{\nu}_p + V\nu_p)\sin\psi_n + (-h\dot{\nu}_y + V\nu_y)\cos\psi_n]\sin\phi \end{aligned} \tag{162}$$

This geometrical angle of attack is written in Fourier series, based upon its past values

$$\alpha_G = \alpha_{G0} + \sum_k \bar{\alpha}_{Gk} e^{i\omega_k t}. \tag{163}$$

For the steady component α_{G0}, the conventional local-circulation method with the Prandtl-Glauert rule is applied, and the following equation is satisfied at each control point:

$$\begin{aligned} l_s &= \frac{1}{2\sqrt{1-M^2}}\rho U^2 c C_{l_\alpha}\left(\alpha_{G0} - \frac{1}{U}\sum \Delta v\right) \\ &= \rho U \sum \Delta\gamma \end{aligned} \tag{164}$$

where Δv and $\Delta\gamma$ are the induced velocity perpendicular to local airflow and the circulation of the hypothetical wing, respectively.

The sinusoidal component of the air loading is given by two-dimensional theory, without considering the effect of compressibility, but with corrections, similar to the wing-air loading case, for aspect ratio and spanwise location:

$$\bar{l}_k = \frac{\eta}{2}\rho U^2 c C_{l\alpha} C\left(\frac{\omega_k c_w}{2V}\right)\bar{\alpha}_{Gk} e^{i\omega_k t} \tag{165}$$

$$\eta = \eta_1 \eta_2 \tag{166}$$

$$\eta_1 = \frac{A}{2 + \sqrt{4 + A^2}} \tag{167}$$

$$\eta_2 = \frac{4}{\pi}\sqrt{1 - \xi^2} \tag{168}$$

$$A = \frac{R - R_c}{c} \tag{169}$$

$$\xi = \frac{2r - (R + R_c)}{R - R_c} \tag{170}$$

Theodorsen's theory treats both the pitching motion and the heaving motion of a wing. The relative velocity of the blade to the air varies along the chordwise position because of pitching motion. Since the rotor blade model does not have a pitching degree of freedom, virtual-mass terms are assumed to be related to the acceleration of the blade elastic axis neglecting blade pitch motion.

$$l_v = \rho\pi \left(\frac{c}{2}\right)^2 (\ddot{w}\cos\phi - \ddot{v}\sin\phi) \tag{171}$$

This equation concludes the air loading calculation. The virtual work required to complete the equations of motion can now be calculated by equations (27) through (29). Timewise integration is carried out using a Runge-Kutta-Gill method. By conducting timewise calculations both with and without the feedback system, the effectiveness of the feedback system can be evaluated.

NUMERICAL RESULTS

The methods of control law determination and the timewise calculation just given are applied in this section. The specifications of the model aircraft used in numerical calculations are given in table 1 and in figures 7 and 8. Blade pitch angle is chosen to give the thrust of 7,000 N at the design advance ratio $V/\Omega R = 0.7$ and such that the thrust changes proportionally to the square of cruising speed. Trim thrust and pitch angle determined in this way are given in figure 9.

Figure 10 presents the change of the real part of the eigenvalues as a function of aircraft cruise velocity. This figure shows that this model remains stable for advance ratios up to 1.8.

To investigate the feedback-control efficiency, the stiffness of the considered tilt-rotor model is reduced. Because flutter peculiar to the tilt-rotor aircraft is the major concern in this report, the wing stiffness was reduced to one-eighth of the baseline model for all the degrees of freedom in the wing, while the rotor-blade stiffness is assumed to be unchanged. Natural frequencies and mode shapes employed in the eigenvalue analysis are given in Figures 11 through 15 for the new rotor/wing model. These modes are attributed to blade-in-plane, blade out-of-plane, wing-upward, wing-forward, and wing-torsional degrees of freedom, respectively. Figure 16 gives the real part of the eigenvalue as a function of advance ratio $V/\Omega R$ for the reduced stiffness model. An eigenvalue will become unstable when the advance ratio exceeds about 1.5.

For further numerical results, an almost critical case in which the advanced ratio is equal to 1.5 is chosen and the design of a control law is investigated. In the previous section, input to the feedback system as a function of wingtip upward and forward bending and torsion was described. Using all of these parameters is not necessary in the present case. When selecting one or more of the parameters, the eigenvector and mode shape corresponding to the unstable mode is of greatest importance. The two eigenvectors which have the greatest real part at the advance ratio of 1.5 are given in figure 17. Among the elements of the eigenvector, only the elements which have absolute values of more than 5% of the largest element value are shown in this figure. The critical element is attributed to the wing's second lowest natural frequency and the other element to the the wing's third lowest frequency. Wing second and third modes correspond, in turn, to forward deflection and torsion, respectively, as seen in Figures 14 and 15. To stabilize or to augment the stability of these modes, feedback of dominant deformations are expected to be effective. As the simplest case, paying attention to the least damped mode only, velocity of the wing forward bending $\dot{w}_w$ is chosen as an input for the feedback system, which means all the feedback gains except for K_{wsd} and K_{wcd} are equal to zero.

Figure 18 shows the effect of feedback on the real part of the systems eigenvalues. Only those eigenvalues that have a real part greater than -1.0 are shown among the eigenvalues, since highly damped modes need not be considered. The imaginary parts (frequency) of the eigenvalues change at most 2% when the feedback gain changes from 0.0 to -0.05. The eigenvalues without feedback are given along each line. The dominant, generalized coordinate corresponding to each eigenvector is also given along each line in parentheses. All the modes are simultaneously stabilized when feeding back the cosine term of cyclic pitch. Some modes are stabilized yet others are destabilized in case of feedback with the sine term of cyclic pitch. Feedback of the sine term of cyclic pitch works about as well as that of the cosine term as far as the critical mode (a_2, wing forward bending) is concerned. However, sine feedback is unfavorable, in that the two modes which have the largest eigenvalue real part cannot be stabilized simultaneously. From figure 18, feedback of the cosine term of cyclic pitch is expected to work better than the sine term of cyclic pitch does. Consequently the feedback gain to the cosine term K_{wcd} is set to -0.03 for evaluation of this control system.

Timewise calculation are made to see whether the feedback system just discussed is effective. Calculations are carried out without introducing rotor-blade or wing elasticity for the first five revolutions of the rotor rotation to get the air loading in an almost equilibrium state. The full equations of motion are employed after five revolutions; thus, the initial conditions for these equations are the deviations from the deflected equilibrium state. Figures 19 through 24 show the results for all the degrees of freedom both without and with feedback control. The abscissa is the number of rotor revolutions after elasticity

is introduced. The results for 100 revolutions, or approximately 15 sec, are given. With no feedback control, the wing-upward deflection appears to be converging (figure 19) because the lowest damped modes are dominated by generalized coordinates a_2 and a_3 (wing-forward deflection and wing torsion). Wing-forward deflection (figure 20) and wing torsion (pylon-pitch angle; figure 21) show oscillation with almost constant amplitude with no feedback. Blade deformations do not appear to converge without control in spite of the fact that the lowest damped modes are not characterized by blade deflection.

Once feedback control is introduced ($\dot{w}_w$ feedback with $k_{wcd} = -0.03$) wing-forward and wing-torsional deflections are stabilized (Figs. 20 and 21). Stabilization is expected because these deflections are characterized by the two lowest damped eigenvalues and the real parts of each value are significantly reduced (stabilized) with the introduction of feedback control. The wing-upward deflection does not show an improvement because the eigenvalue, characterizing this motion ($\omega = 6.0\ rad/sec$) is not affected by the introduction of feedback to the cosine term. The amplitude of blade-out-of-plane deflection becomes smaller since the eigenvalue for that mode ($\omega = 62.3\ rad/sec$) is changed by the control. The cyclic-pitch angle (figure 24) is sufficiently small so that there is additional control capability for stabilizing less stable flight conditions or for stabilizing oscillations of greater amplitude. From this time-history analysis, this control system has been proved to work as it should, and it would be expected to work as well under less stable operating conditions.

CONCLUDING REMARKS

Tilt rotor flutter control was investigated. The determination of the control law was based on a harmonic-balance method using a simple aerodynamic theory. It was confirmed that the stability of tilt-rotor motion is improved by using closed-loop, cyclic-pitch control. The validity of the control law determined in this way was demonstrated by a timewise calculation in which more sophisticated aerodynamics were considered. The selection of the feedback gain and the placement of the sensor were not based on any specific criterion. Establishing the optimal gain is left to future study.

APPENDIX A

Expressions for K^i_{Wnj}, K^i_{Bnj}, K^i_S, K^i_C and K^i_0

Rotor-blade loading $p_{\theta n}$ and p_{zn} are expressed in harmonic terms.

$$p_{\theta n} = p_{\theta 0} + p_{\theta s}\sin\psi_n + p_{\theta c}\cos\psi_n$$

$$p_{zn} = p_{z0} + p_{zs}\sin\psi_n + p_{zc}\cos\psi_n$$

Moreover the variables $p_{\theta 0}$, $p_{\theta s}$, $p_{\theta c}$, p_{z0}, p_{zs}, and p_{zc} are subdivided into pitch-angle and generalized-coordinate terms:

$$\begin{aligned}
p_{\theta n} =& p_{\theta 00} + \sum_{j=1}^{2} p_{\theta 0\dot{q}_{j0}}\dot{q}_{j0} + \sum_{j=1}^{3} p_{\theta 0\dot{a}_j}\dot{a}_j \\
&+ \Big(p_{\theta ss}\theta_s + \sum_{j=1}^{2} p_{\theta s\dot{q}_{j*}}\dot{q}_{js} + \sum_{j=1}^{2} p_{\theta sq_{jc}}q_{jc} \\
&\quad + \sum_{j=1}^{3} p_{\theta s\dot{a}_j}\dot{a}_j + \sum_{j=1}^{3} p_{\theta sa_j}a_j\Big)\sin\psi_n \\
&+ \Big(p_{\theta cc}\theta_c + \sum_{j=1}^{2} p_{\theta c\dot{q}_{jc}}\dot{q}_{jc} + \sum_{j=1}^{2} p_{\theta cq_{j*}}q_{js} \\
&\quad + \sum_{j=1}^{3} p_{\theta c\dot{a}_j}\dot{a}_j + \sum_{j=1}^{3} p_{\theta ca_j}a_j\Big)\cos\psi_n \\
p_{zn} =& p_{z00} + \sum_{j=1}^{2} p_{z0\dot{q}_{j0}}\dot{q}_{j0} + \sum_{j=1}^{3} p_{z0\dot{a}_j}\dot{a}_j \\
&+ \Big(p_{zss}\theta_s + \sum_{j=1}^{2} p_{zs\dot{q}_{j*}}\dot{q}_{js} + \sum_{j=1}^{2} p_{zsq_{jc}}q_{jc} \\
&\quad + \sum_{j=1}^{3} p_{zs\dot{a}_j}\dot{a}_j + \sum_{j=1}^{3} p_{zsa_j}a_j\Big)\sin\psi_n \\
&+ \Big(p_{zcc}\theta_c + \sum_{j=1}^{2} p_{zc\dot{q}_{jc}}\dot{q}_{jc} + \sum_{j=1}^{2} p_{zcq_{j*}}q_{js} \\
&\quad + \sum_{j=1}^{3} p_{zc\dot{a}_j}\dot{a}_j + \sum_{j=1}^{3} p_{zca_j}a_j\Big)\cos\psi_n
\end{aligned}$$

where

$$p_{\theta 00} = -\frac{1}{2\sqrt{1-M^2}}\rho V_R^2 c C_{l\alpha}(\theta_0 - \phi)\sin\phi - \frac{1}{2}\rho V_R^2 c C_d \cos\phi$$

$$p_{\theta 0\dot{q}_{j0}} = -\frac{1}{2\sqrt{1-M^2}}\rho V_R^2 c C_{l\alpha}\frac{S_{B1j}}{V_R}\sin\phi$$

$$p_{\theta 0\dot{a}_j} = -\frac{1}{2\sqrt{1-M^2}}\rho V_R^2 c C_{l\alpha}\frac{S_{W1j}}{V_R}\sin\phi$$

$$p_{\theta ss} = -\frac{1}{2\sqrt{1-M^2}}\rho V_R^2 c C_{l\alpha}\sin\phi$$

$$p_{\theta s\dot{q}_{j*}} = -\frac{1}{2\sqrt{1-M^2}}\rho V_R^2 c C_{l\alpha}\frac{S_{B2j}}{V_R}\sin\phi$$

$$p_{\theta sq_{jc}} = -\frac{1}{2\sqrt{1-M^2}}\rho V_R^2 c C_{l\alpha}\frac{S_{B3j}}{V_R}\sin\phi$$

$$p_{\theta s\dot{a}_j} = -\frac{1}{2\sqrt{1-M^2}}\rho V_R^2 c C_{l\alpha}\frac{S_{W2j}}{V_R}\sin\phi$$

$$p_{\theta sa_j} = -\frac{1}{2\sqrt{1-M^2}}\rho V_R^2 c C_{l\alpha}\frac{S_{W3J}}{V_R}\sin\phi$$

$$p_{\theta cc} = -\frac{1}{2\sqrt{1-M^2}}\rho V_R^2 c C_{l\alpha}\sin\phi$$

$$p_{\theta c\dot{q}_{jc}} = -\frac{1}{2\sqrt{1-M^2}}\rho V_R^2 c C_{l\alpha}\frac{S_{B4j}}{V_R}\sin\phi$$

$$p_{\theta cq_{j*}} = -\frac{1}{2\sqrt{1-M^2}}\rho V_R^2 c C_{l\alpha}\frac{S_{B5j}}{V_R}\sin\phi$$

$$p_{\theta c\dot{a}_j} = -\frac{1}{2\sqrt{1-M^2}}\rho V_R^2 c C_{l\alpha}\frac{S_{W4j}}{V_R}\sin\phi$$

$$p_{\theta ca_j} = -\frac{1}{2\sqrt{1-M^2}}\rho V_R^2 c C_{l\alpha}\frac{S_{W5j}}{V_R}\sin\phi$$

$$p_{z00} = \frac{1}{2\sqrt{1-M^2}}\rho V_R^2 c C_{l\alpha}(\theta_0 - \phi)\cos\phi - \frac{1}{2}\rho V_R^2 c C_d \sin\phi$$

$$p_{z0\dot{q}_{j0}} = \frac{1}{2\sqrt{1-M^2}}\rho V_R^2 c C_{l\alpha}\frac{S_{B1j}}{V_R}\cos\phi$$

$$p_{z0\dot{a}_j} = \frac{1}{2\sqrt{1-M^2}}\rho V_R^2 c C_{l\alpha}\frac{S_{W1j}}{V_R}\cos\phi$$

$$p_{zss} = \frac{1}{2\sqrt{1-M^2}}\rho V_R^2 c C_{l\alpha}\cos\phi$$

$$p_{zs\dot{q}_{js}} = \frac{1}{2\sqrt{1-M^2}}\rho V_R^2 c C_{l\alpha}\frac{S_{B2j}}{V_R}\cos\phi$$

$$p_{zsq_{jc}} = \frac{1}{2\sqrt{1-M^2}}\rho V_R^2 c C_{l\alpha}\frac{S_{B3j}}{V_R}\cos\phi$$

$$p_{zs\dot{a}_j} = \frac{1}{2\sqrt{1-M^2}}\rho V_R^2 c C_{l\alpha}\frac{S_{W2j}}{V_R}\cos\phi$$

$$p_{zsa_j} = \frac{1}{2\sqrt{1-M^2}}\rho V_R^2 c C_{l\alpha}\frac{S_{W3J}}{V_R}\cos\phi$$

$$p_{zcc} = \frac{1}{2\sqrt{1-M^2}}\rho V_R^2 c C_{l\alpha}\cos\phi$$

$$p_{zc\dot{q}_{jc}} = \frac{1}{2\sqrt{1-M^2}}\rho V_R^2 c C_{l\alpha}\frac{S_{B4j}}{V_R}\cos\phi$$

$$p_{zcq_{js}} = \frac{1}{2\sqrt{1-M^2}}\rho V_R^2 c C_{l\alpha}\frac{S_{B5j}}{V_R}\cos\phi$$

$$p_{zc\dot{a}_j} = \frac{1}{2\sqrt{1-M^2}}\rho V_R^2 c C_{l\alpha}\frac{S_{W4j}}{V_R}\cos\phi$$

$$p_{zca_j} = \frac{1}{2\sqrt{1-M^2}}\rho V_R^2 c C_{l\alpha}\frac{S_{W5j}}{V_R}\cos\phi$$

Substituting these relations into equation (29) yields

$$f_i = \sum_{j=1}^{3}\left(K^i_{W1j}\dot{a}_j + K^i_{W2j}a_j\right)$$
$$+\sum_{j=1}^{2}\left(K^i_{B1j}\dot{q}_{j0} + K^i_{B2j}q_{j0} + K^i_{B3j}\dot{q}_{js} + K^i_{B4j}q_{js} + K^i_{B5j}\dot{q}_{jc} + K^i_{B6j}q_{jc}\right)$$
$$+K^i_S\theta_s + K^i_C\theta_c + K^i_0$$

$$K^i_{W1j} = \frac{N}{2}\int_0^R \Big[- X_i p_{\theta s\dot{a}_j} + 2Z_i p_{z0\dot{a}_j}$$
$$+ N_{yi}(-hp_{\theta c\dot{a}_j} + rp_{zs\dot{a}_j})$$
$$- N_{pi}(hp_{\theta s\dot{a}_j} + rp_{zc\dot{a}_j})$$
$$+ 2N_{ri}rp_{\theta 0\dot{a}_j}\Big]\,dr$$

$$K^i_{W2j} = \frac{N}{2}\int_0^R \big[X_i(-p_{\theta sa_j} + 2N_{yj}p_{z00}) + N_{yi}(-hp_{\theta ca_j} + rp_{zsa_j} + 2rN_{pj}p_{\theta 00}) + N_{pi}(-2N_{yj}p_{\theta 00} - hp_{\theta sa_j} - hp_{zca_j})\big]\,dr$$

$$K^i_{B1j} = \frac{N}{2}\int_0^R \big(2Z_i p_{z0\dot{q}_{j0}} + 2N_{ri}rp_{\theta 0\dot{q}_{j0}}\big)\,dr$$

$$K^i_{B2j} = \frac{N}{2}\int_0^R \big(-X_i p_{\theta sq_{j*}} + N_{yi}rp_{zs\dot{q}_{j*}} - N_{pi}hp_{\theta s\dot{q}_{j*}}\big)\,dr$$

$$K^i_{B3j} = \frac{N}{2}\int_0^R \big(-N_{yi}hp_{\theta c\dot{q}_{jc}} - N_{pi}rp_{zc\dot{q}_{jc}}\big)\,dr$$

$$K^i_{B4j} = 0$$

$$K^i_{B5j} = \frac{N}{2}\int_0^R \big[-X_i p_{\theta sq_{j*}} + N_{yi}(-hp_{\theta cq_{j*}} + rp_{zsq_{j*}}) + N_{pi}(V_j p_{z00} - W_j p_{\theta 00} - rp_{zcq_{j*}} - hp_{\theta sq_{j*}})\big]\,dr$$

$$K^i_{B6j} = \frac{N}{2}\int_0^R \big[-X_i p_{\theta sq_{jc}} + N_{yi}(V_j p_{z00} - W_j p_{\theta 00} + rp_{zsq_{jc}} - hp_{\theta cq_{jc}}) - N_{pi}(hp_{\theta sq_{jc}} + rp_{zcq_{jc}})\big]\,dr$$

$$K^i_S = \frac{N}{2}\int_0^R \big(-X_i p_{\theta ss} + N_{yi}rp_{zss} - N_{pi}hp_{\theta ss}\big)\,dr$$

$$K^i_C = \frac{N}{2}\int_0^R \big(-N_{yi}hp_{\theta cc} - N_{pi}rp_{zcc}\big)\,dr$$

$$K^i_0 = N\int_0^R \big(Z_i p_{z00} + N_{ri}rp_{\theta 00}\big)\,dr$$

APPENDIX B

Matrix Elements of Final Equations

The following matrix elements for equations (112) through (114), with an exception for $E^2_{i,i}$, are given for: $i = 1,2$; $j = 1,2$; $k = 1,3$; and $l = 1,3$:

$$E^2_{i,i} = 1 \quad (i = 1 \sim 9)$$
$$E^2_{3i-2,k+6} = Q^i_{1k}$$
$$E^2_{3i-1,k+6} = Q^i_{2k}$$
$$E^2_{3i,k+6} = Q^i_{4k}$$
$$E^2_{k+6,3i-2} = NA^i_{1k}$$
$$E^2_{k+6,3i-1} = \frac{N}{2}A^k_{2i}$$
$$E^2_{k+6,3i} = \frac{N}{2}A^k_{3i}$$

$$E^1_{3i-2,3j-2} = -I^i_{B1j}$$
$$E^1_{3i-2,k+6} = -I^i_{W1k}$$
$$E^1_{3i-1,3j-1} = -I^i_{B2j}$$
$$E^1_{3i-1,3i} = -2\Omega$$
$$E^1_{3i-1,k+6} = Q^i_{3k} - I^i_{W2k}$$
$$E^1_{3i,3i-1} = 2\Omega$$
$$E^1_{3i,3j} = -I^i_{B4j}$$
$$E^1_{3i,k+6} = Q^i_{5k} - I^i_{W4k}$$
$$E^1_{k+6,3i-2} = -K^k_{B1i}$$
$$E^1_{k+6,3i-1} = \frac{N}{2}A^k_{4i} + N\Omega A^k_{3i} - K^k_{B2i}$$
$$E^1_{k+6,3i} = \frac{N}{2}A^k_{5i} - N\Omega A^k_{2i} - K^k_{B4i}$$
$$E^1_{k+6,l+6} = I_B N\Omega(N_{yk}N_{pl} - N_{pl}N_{yk}) - G^k_{W3l} - K^k_{W1l}$$

$$E^0_{3i-2,3i-2} = \omega_i^2$$
$$E^0_{3i-1,3i-1} = \omega_i^2 - \Omega^2$$
$$E^0_{3i-1,3j} = -I^i_{B3j}$$
$$E^0_{3i-1,k+6} = -I^i_{W3k}$$
$$E^0_{3i,3j-1} = -I^i_{B5j}$$
$$E^0_{3i,3i} = \omega_i^2 - \Omega^2$$
$$E^0_{3i,k+6} = -I^i_{W5k}$$
$$E^0_{k+6,3i-2} = K^k_{B4i}$$
$$E^0_{k+6,3i-1} = \frac{N}{2}(A^k_{6i} + \Omega A^k_{5i} - \Omega^2 A^k_{2i}) - K^k_{B5i}$$
$$E^0_{k+6,3i} = \frac{N}{2}(A^k_{7i} - \Omega A^k_{4i} - \Omega^2 A^k_{3i}) - K^k_{B6i}$$
$$E^0_{j+6,k+6} = \begin{cases} -G^j_{W2k} & j \neq k \\ -G^j_{W2k} + \omega^2_{wj} & j = k \end{cases}$$

$$D_{3i-2,1} = I^i_{B0}$$
$$D_{3i-1,2} = I^i_S$$
$$D_{3i,3} = I^i_C$$
$$D_{k+6,1} = K^k_0$$
$$D_{k+6,2} = K^k_S$$
$$D_{k+6,3} = K^k_C$$

$E^n_{i,j}$(if not given above) = 0
$D_{i,j}$(if not given above) = 0

APPENDIX C

Vortex Lattice Method for Wing Aerodynamics

Figure C1 shows the tilt-rotor-wing coordinate system for the bound-vortex calculation. Only the right half wing is shown because the whole wing is assumed to be symmetric. The semispan wing is equally divided into k segments and the vortex $\delta\gamma_i$ is trailed from the outer edge of the ith segment. Downwash at the ith control point v_i is given as

$$v_i = \sum_{j=1}^{k} B_{ij}\delta\gamma_j$$

where $B_{ij}\delta\gamma_j$ is the induced velocity on ith control point by the trailing vortex from the outer edge of jth segment. The wing's mirror image and corresponding bound vortex connects the upper two trailing vortices. The coefficients B_{ij} are given by

$$B_{ij} = \frac{1}{4\pi(y_{bj} - y_{ci})}\left[2 + \frac{x_c + y_{bj} - y_{ci}}{\sqrt{(y_{ci} - y_{bj})^2 + x_c^2}} + \frac{x_c + y_{bj} + y_{ci}}{\sqrt{(y_{ci} + y_{bj})^2 + x_c^2}}\right]$$

where x_c is the distance between the bound vortex and the control point and is equal to the semi-chord, y_{bj} is the distance of jth segment outer edge from the center of whole wing, and y_{ci} is the distance of the ith control point from the center of the whole wing. Writing the boundary condition (i.e., downwash on the ith control point) as b_i, the equation which connects the intensity of each trailing vortex and the boundary conditions is given by

$$(B)\begin{pmatrix} \delta\gamma_1 \\ \delta\gamma_2 \\ \vdots \\ \delta\gamma_k \end{pmatrix} = \begin{pmatrix} b_1 \\ b_2 \\ \vdots \\ b_k \end{pmatrix}$$

$$(B) = \begin{pmatrix} B_{11} & B_{12} & \dots & B_{1k} \\ B_{21} & B_{22} & \dots & B_{2k} \\ \vdots & \vdots & \ddots & \vdots \\ B_{k1} & B_{k2} & \dots & B_{kk} \end{pmatrix}$$

The intensity of the trailing vortex is given by

$$\begin{pmatrix} \delta\gamma_1 \\ \delta\gamma_2 \\ \vdots \\ \delta\gamma_k \end{pmatrix} = (B)^{-1}\begin{pmatrix} b_1 \\ b_2 \\ \vdots \\ b_k \end{pmatrix}$$

The intensity of the bound vortex in the jth section γ_{bj} is

$$\gamma_{bk} = \delta\gamma_k$$
$$\gamma_{b\,k-i} = \gamma_k + \delta\gamma_{k-i} \qquad i = 1, 2, \ldots k-1$$

Finally, the lift distribution in ith section l_i is

$$l_i = \rho V \gamma_{bi}$$

To determine the direction of the lift, the induced velocity on the bound vortex v_{bi} needs to be determined. The lift is caused by the trailing vortex only, since a straight and unswept wing is considered. The equation for the induced velocity is

$$v_{bi} = \frac{1}{4\pi} \sum_{j=1}^{k} \left(\frac{\delta\gamma_j}{y_{bj} - y_{ci}} + \frac{\delta\gamma_j}{y_{bj} + y_{ci}} \right)$$

The backward inclination of lift ϕ_w is given by

$$\phi_w = v_{bi}/V$$
$$= \frac{1}{4\pi V} \sum_{j=1}^{k} \left(\frac{\delta\gamma_j}{y_{bj} - y_{ci}} + \frac{\delta\gamma_j}{y_{bj} + y_{ci}} \right)$$

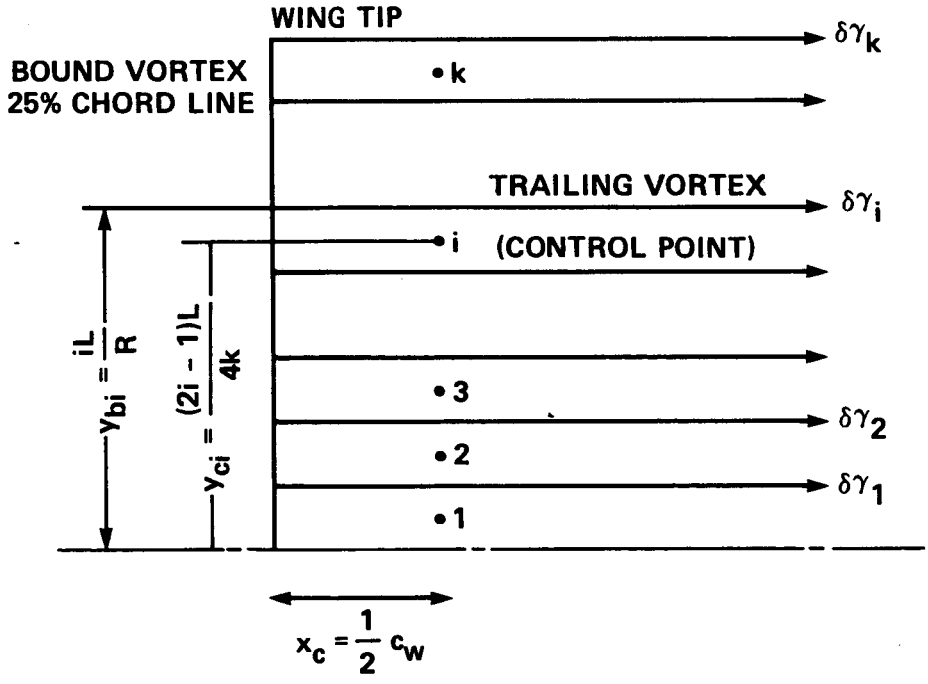

Figure C1.- Vortex lattice geometry for wing aerodynamics.

REFERENCES

1. Yasue, M.: A Study of Gust Responce for a Rotor-Propeller in Cruising Flight. NASA CR-137537, 1974.
2. Nasu, K.: A Method of Computation for the Blade Loading of Rotary Wing. Ph.D. thesis, Univ. of Tokyo, 1983.
3. Azuma, A.; Nasu, K.; and Hayashi T.: An Extension of the Local Momentum Theory to the Rotors Operating in Twisted Flow Field. Vertica, vol.7, no.1, 1983, pp. 45-59.
4. Nasu, K.; and Azuma, A.: An Experimental Verification of the Local Circulation Method for a Horizontal Axis Wind Turbine. Research on Natural Energy, March 1984, pp. 245-252.
5. Saito, S.; Azuma, A.; and Nagao, M.: Gust Response of Rotary Wing Aircraft and Its Alleviation. Vertica, vol.5, no.2, 1981, pp.173-184
6. Johnson, W.: Aeroelastic Analysis for Rotorcraft in Flight or in a Wind Tunnel. NASA TN D-8515, 1977.
7. Cavin, R.K., III; and Dusto, A.R.: Hamilton's principle: Finite-Element Methods and Flexible Body Dynamics. AIAA J., vol. 15, no. 2, Dec. 1977, pp. 1684-1690.
8. Saito, S.: Application of an Adaptive Blade Control Algorithm to a Gust Alleviation System, NASA TM-85848, Sept. 1983.
9. Landgrebe, A.J.; and Davis, M.W.: Analysis of Potential Helicopter Vibration Reduction Concepts. NASA CP-2400, Nov. 1985, pp.343-363.
10. Ham, N.: Helicopter Gust Alleviation, Attitude Stabilization and Vibration Alleviation Using Individual-Blade-Control Through a Conventional Swash Plate. 41st Ann. Forum of Amer. Helicopter Soc., Fort Worth, Texas, May 1985.
11. Straub, F.K.; and Warmbrodt, W.:The Use of Active Controls to Augment Rotor/Fuselage Stability. J. Amer. Helicopter Soc., vol.30, no.3 July 1985, pp 13-22.
12. Bisplinghoff, R.L.; Ashley, H.; and Halfman, R.L.: Aeroelasticity. Addison-Wesley Publishing Company Inc., 1955

TABLE 1.- SPECIFICATION OF BASELINE TILT ROTOR MODEL.

ROTOR	
number of blades, N	3
radius, R	3.81 m
cutout, R_c	0.15R
chord, c	0.356 m
solidity, σ	0.076
lift slope, $C_{l\alpha}$	5.73
drag coefficient, C_d	0.0125
rotational angular velocity, Ω	40.4 rad/sed (386.0 rpm)
blade-flapping inertia, I_B	176.1 kg · m^2
blade mass, M_B	42.9 kg
WING	
semispan, L	5.08 m
chord, c_w	1.58 m
geometric angle of attack, α_W	2.7°
lift slope, $C_{l\alpha}$	5.73
drag coefficient, c_d	0.004
pitching moment coefficient, C_m	−0.005
position of elastic axis from leading edge, a_e	0.26
position of center of gravity from leading edge, c_g	0.26
PYLON	
mass, M_P	644.0 kg
mast height, h	1.3 m
pitching mass moment of inertia, I_{pp}	257.6 kg · m^2
rolling mass moment of inertia, I_{pr}	57.5 kg · m^2
yawing mass moment of inertia, I_{py}	223.4 kg · m^2

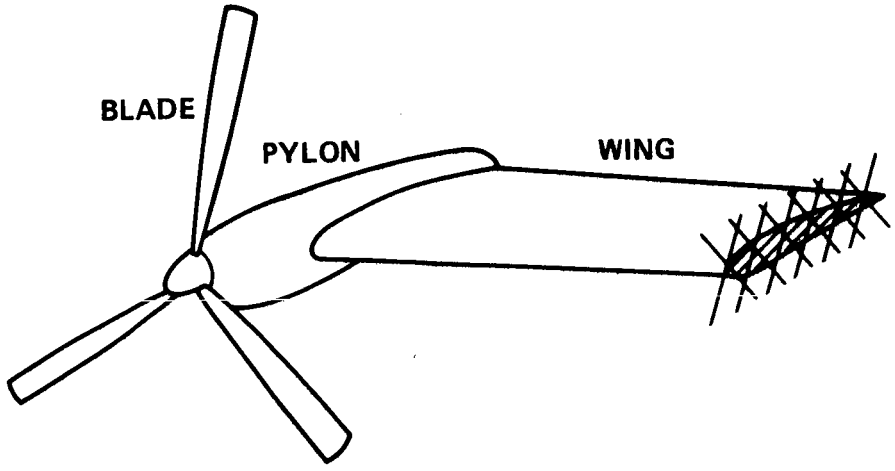

Figure 1.- Tilt-rotor model.

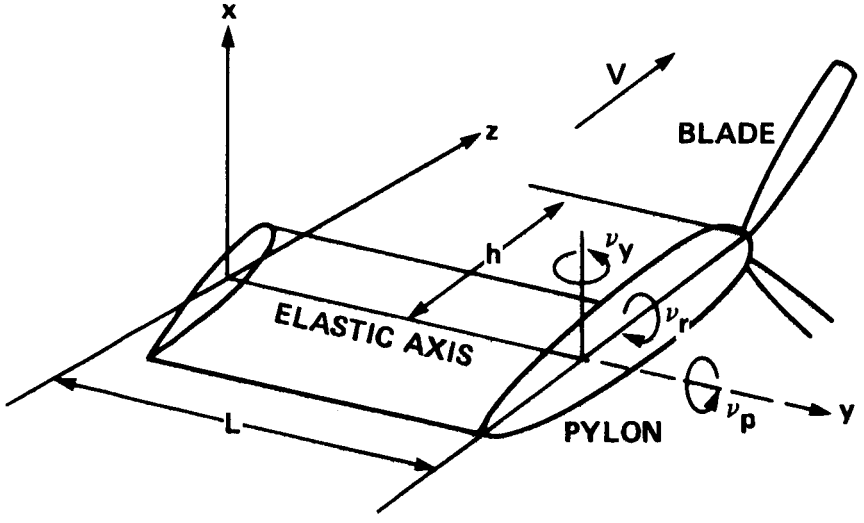

Figure 2.- Coordinate system and pylon rotations.

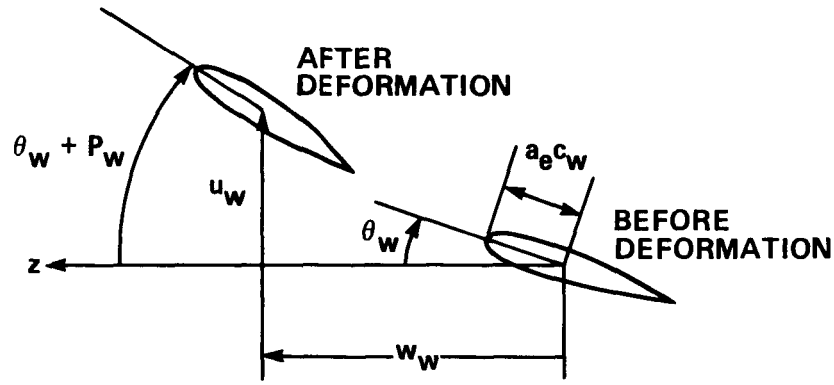

a.- Wing.

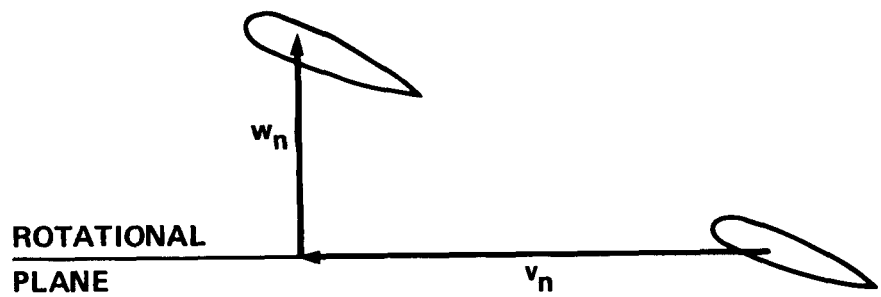

b.- Blade.

Figure 3.- Wing and blade deformation.

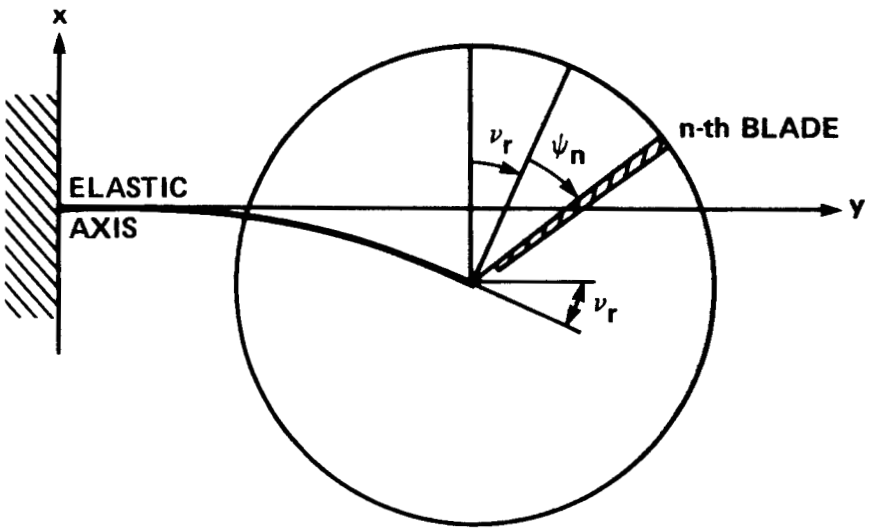

Figure 4.- Rotor azimuth angle and pylon rotation.

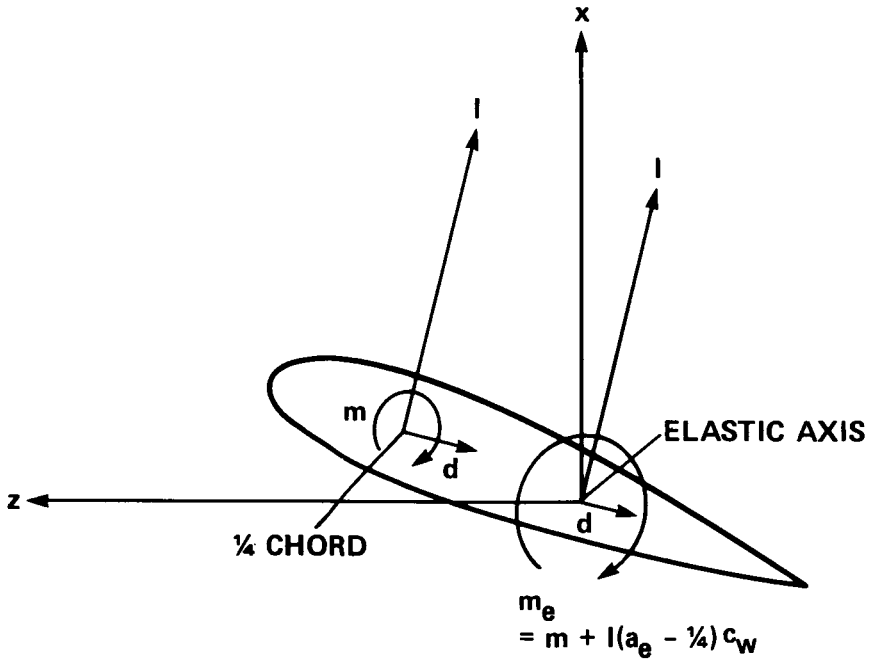

a.- Wing.

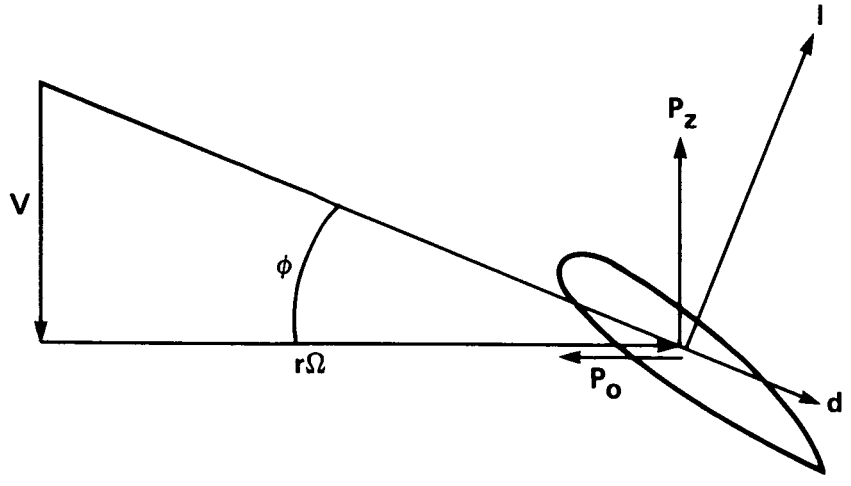

b.- Blade.

Figure 5.- Air-loading geometry on wing and blade.

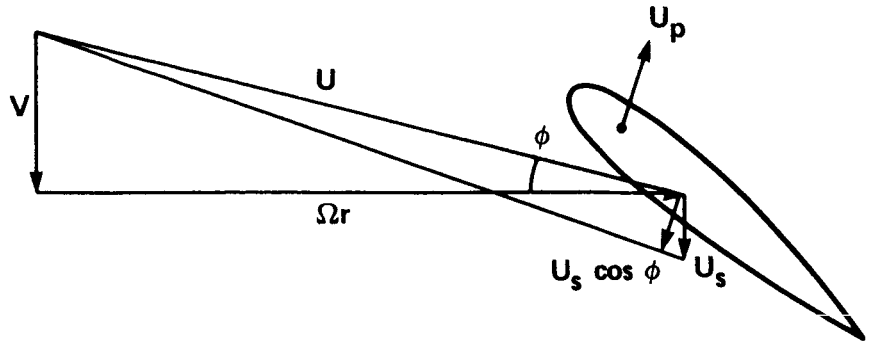

Figure 6.- Airflow and blade motion geometry.

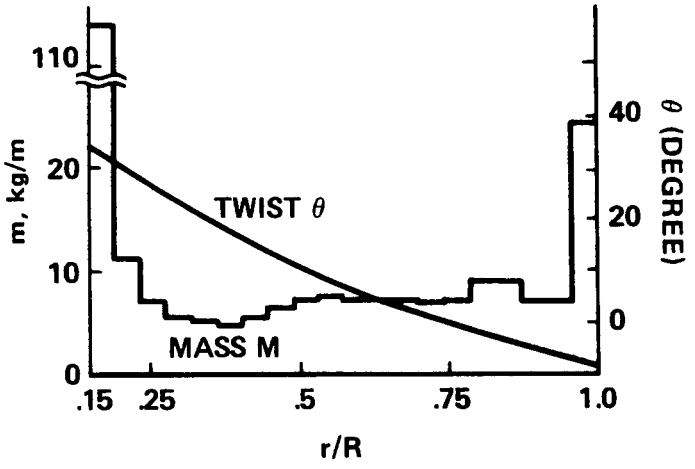

a.- Mass and twist.

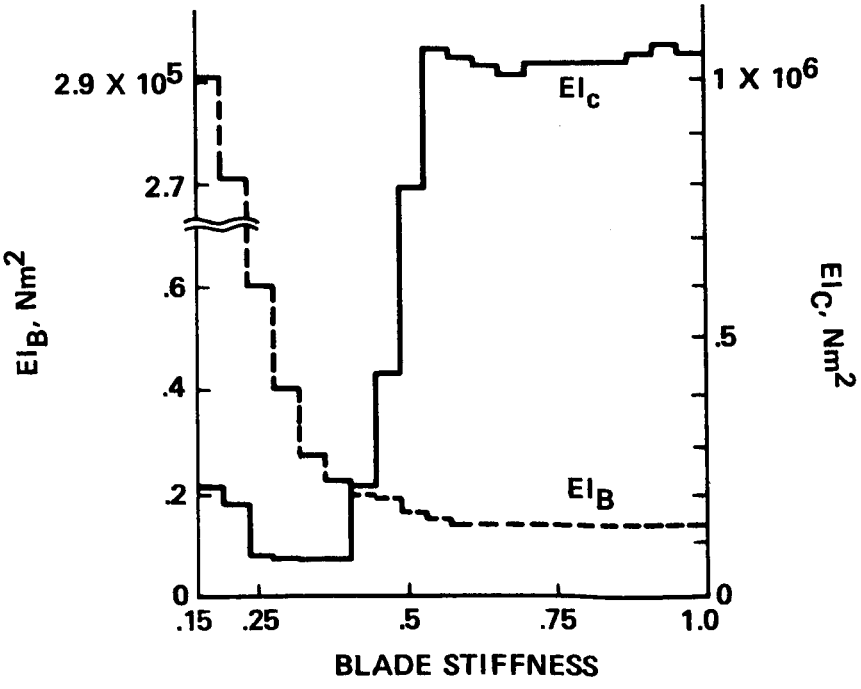

b.- Stiffness.

Figure 7.- Blade structural properties.

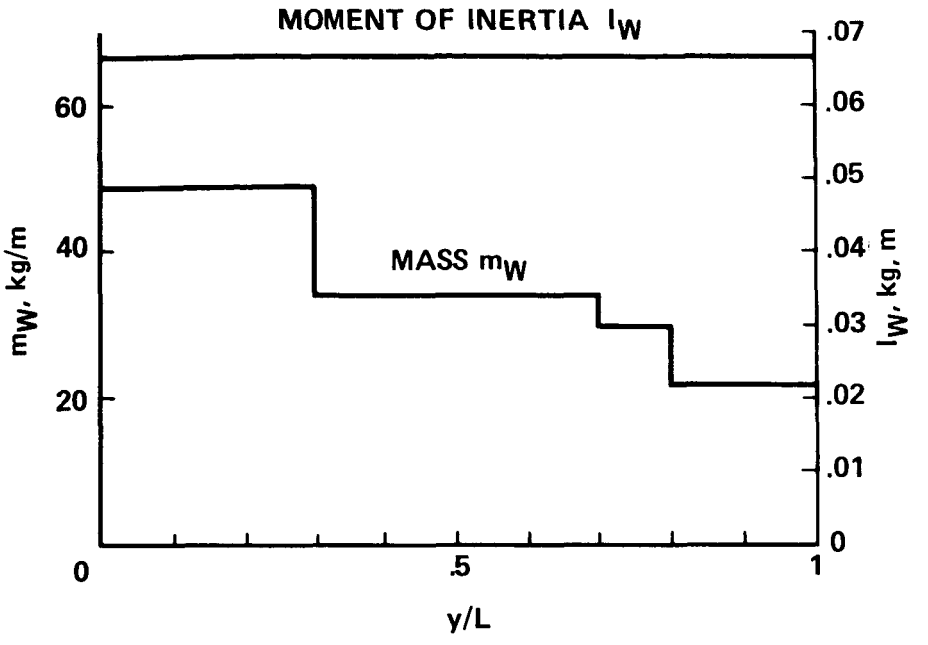

a.- Mass and moment of inertia.

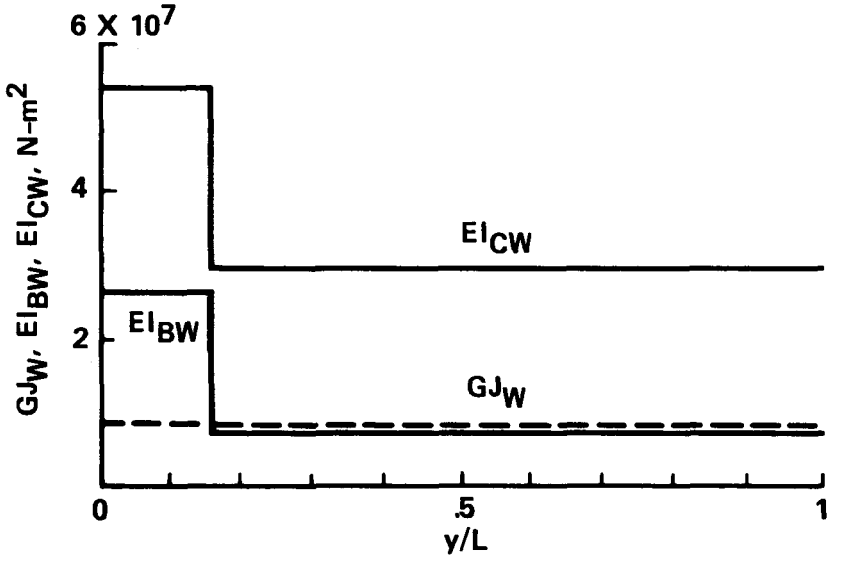

b.- Stiffness.

Figure 8.- Baseline-wing structural properties.

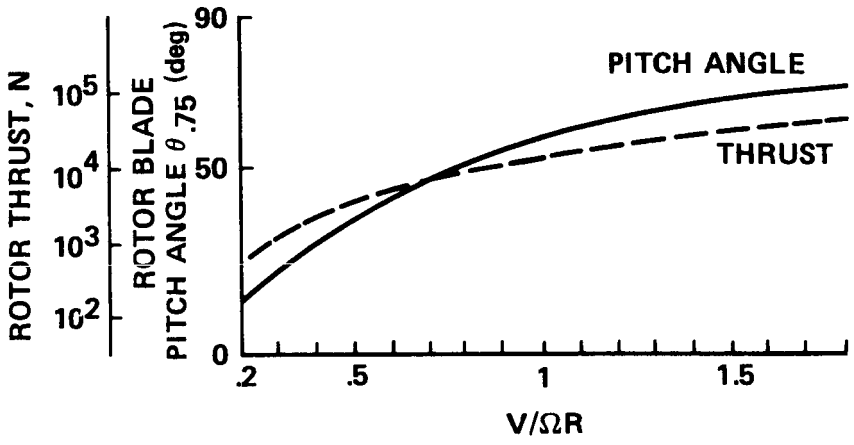

Figure 9.- Pitch angle and thrust necessary for cruise flight.

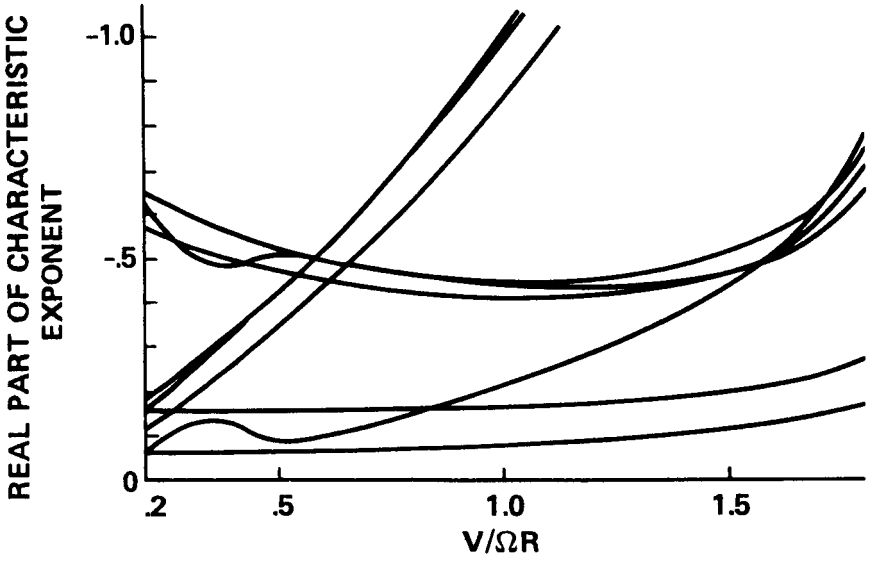

Figure 10.- Real part of eigenvalues for baseline-wing configuration.

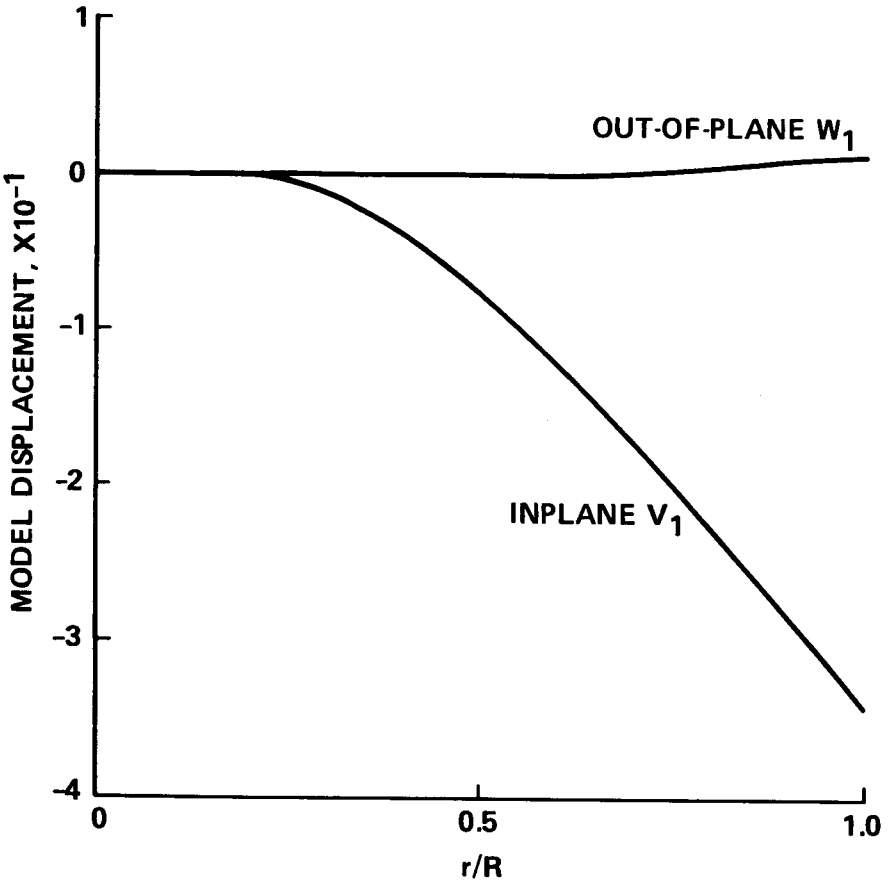

Figure 11.- First blade mode shape; $\omega_1 = 37.6$ rad/sec.

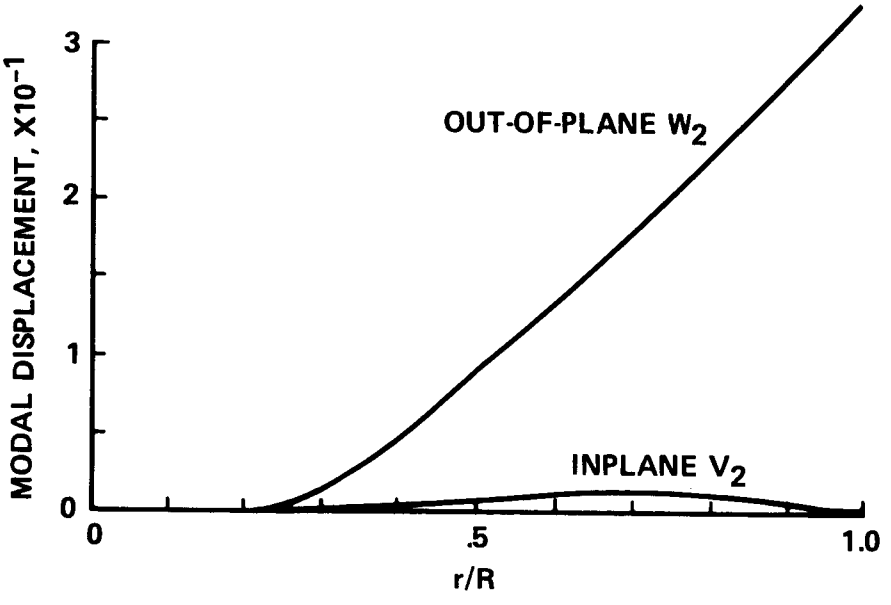

Figure 12.- Second blade mode shape; $\omega_2 = 60.6$ rad/sec.

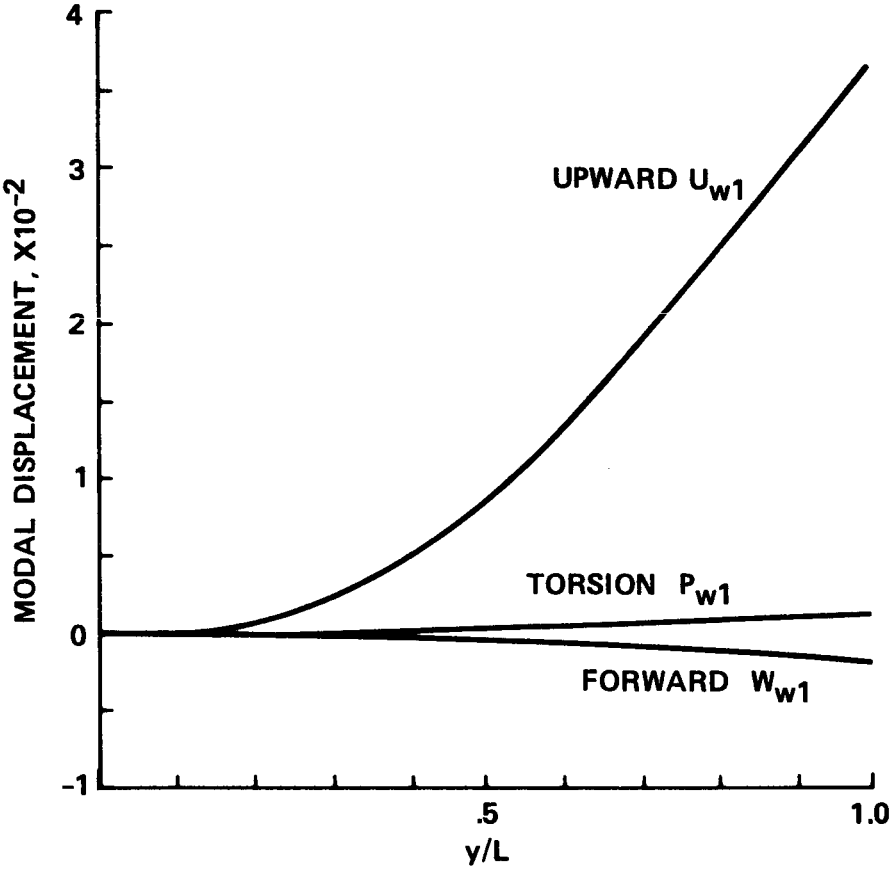

Figure 13.- First wing mode shape; $\omega_{w1} = 6.19$ rad/sec.

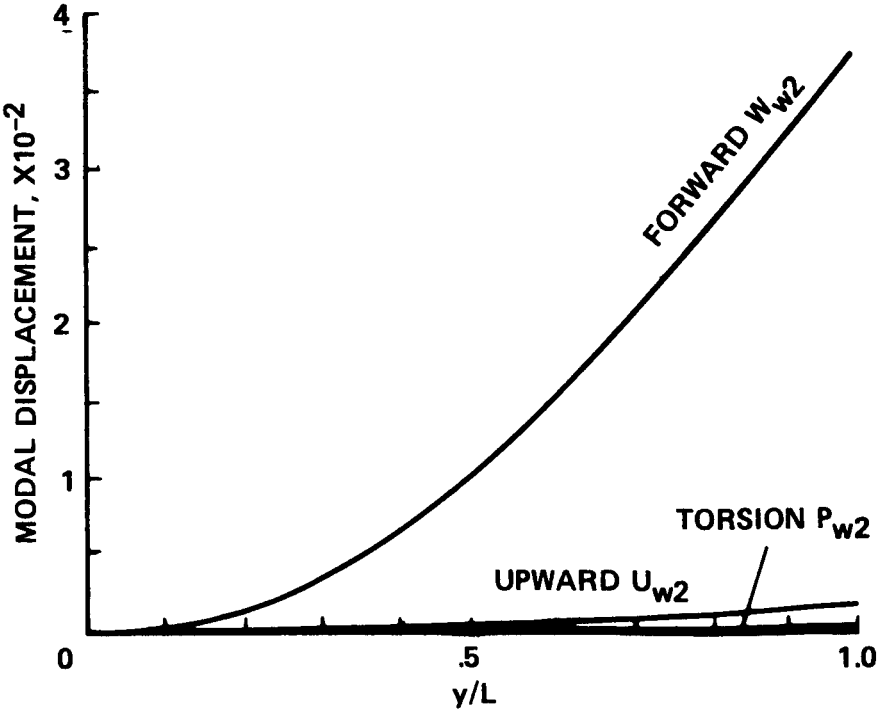

Figure 14.- Second wing mode shape; $\omega_{w2} = 11.2$ rad/sec.

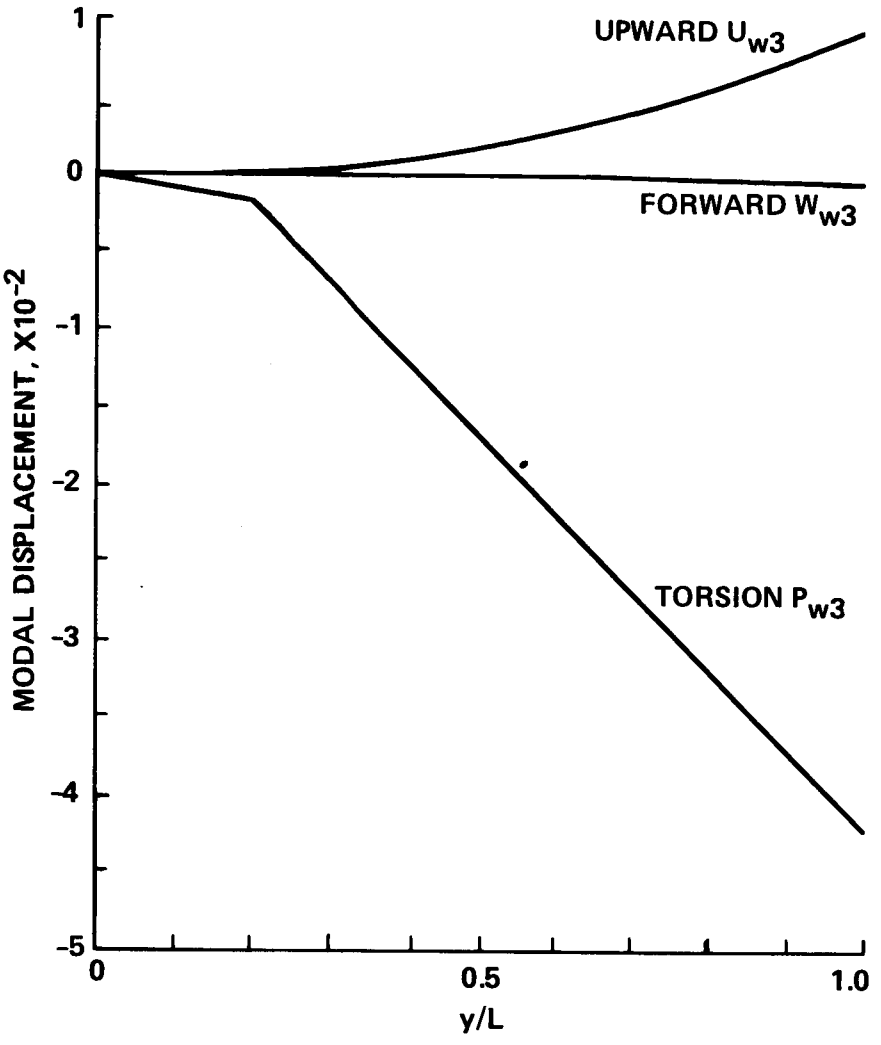

Figure 15.- Third wing mode shape; $\omega_{w3} = 18.1$ rad/sec.

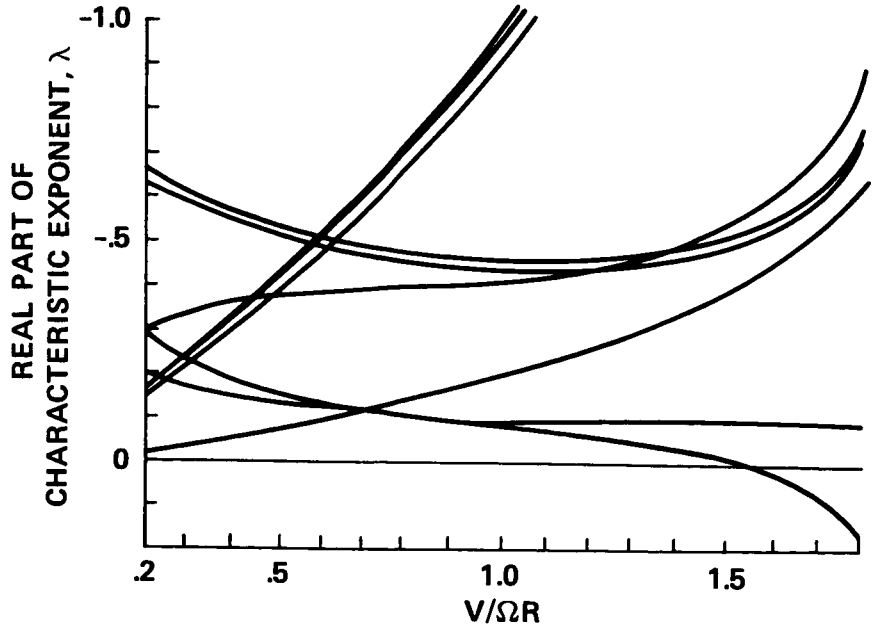

Figure 16.- Real part of eigenvalues for one eighth stiffness wing configuration.

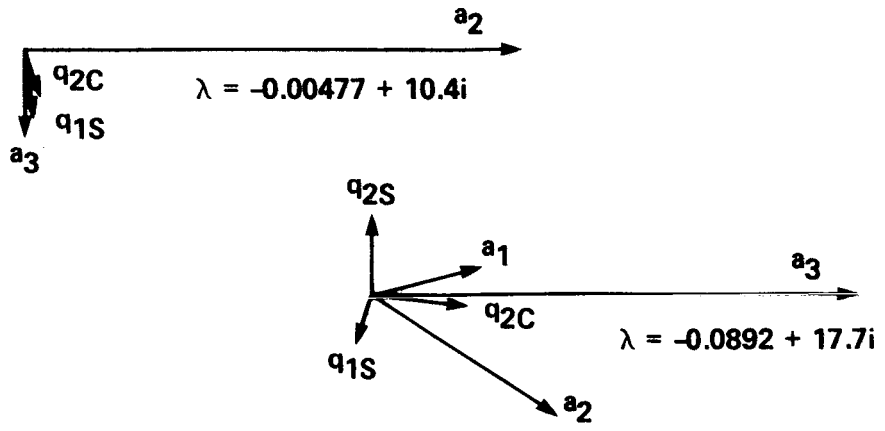

Figure 17.- Eigenvectors without feedback for lowest damped modes; $V/\Omega R = 1.5$.

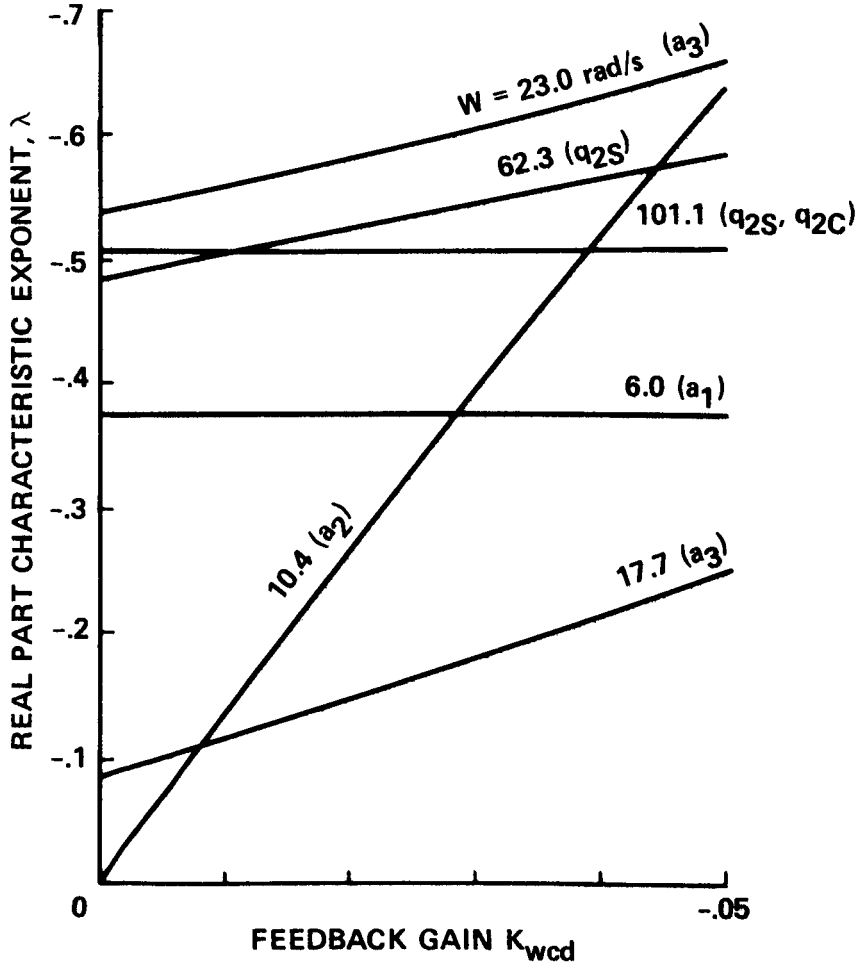

a.- Cosine cyclic feedback; K_{wcd}.

Figure 18.- Real part of eigenvalues with wing feedback; $V/\Omega R = 1.5$.

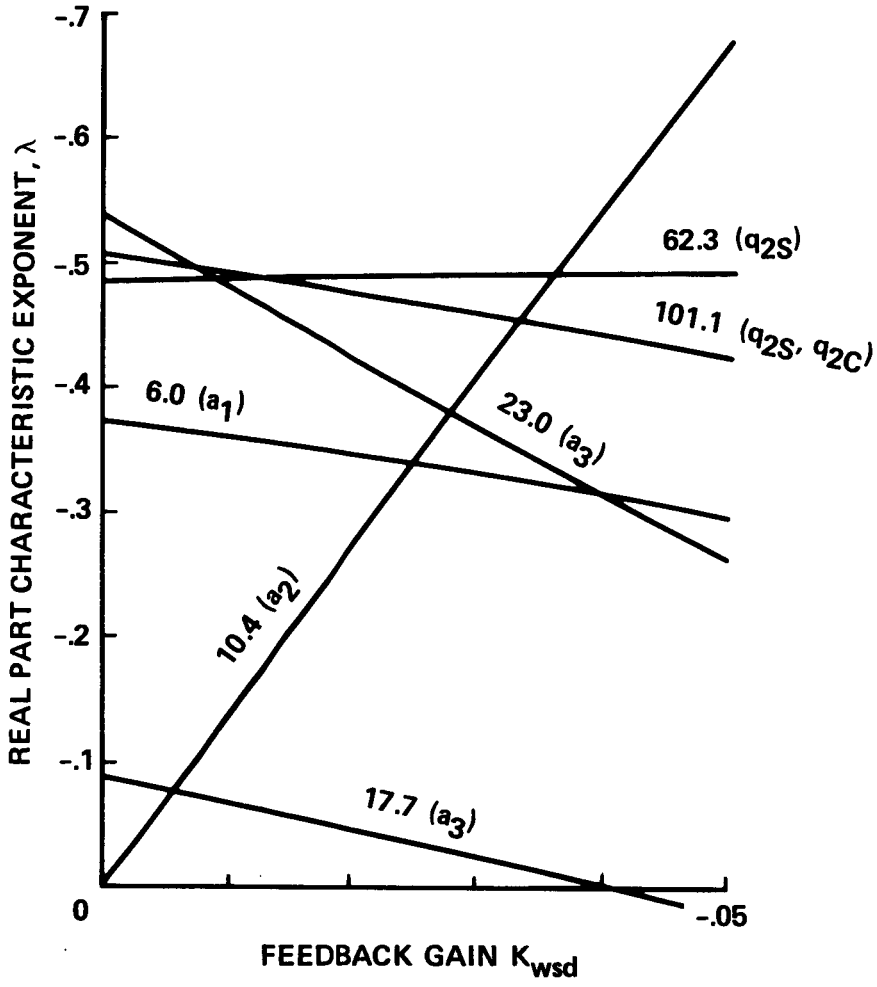

b.- Sine cyclic feedback; K_{wsd}.

Figure 18.- Concluded.

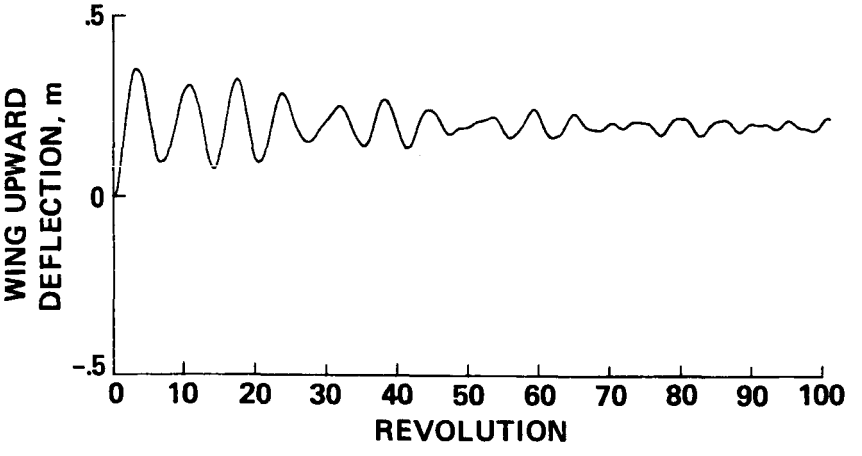

a.- No feedback control.

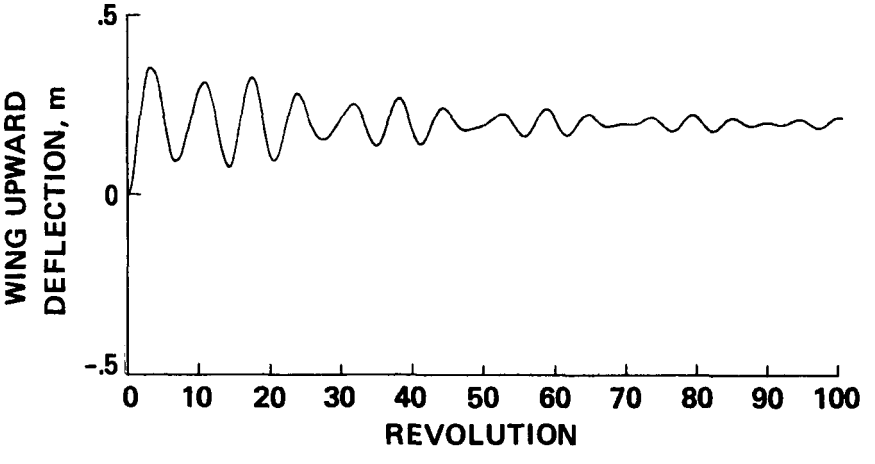

b.- Feedback control; $K_{wcd} = -0.03$.

Figure 19.- Wingtip upward deflection.

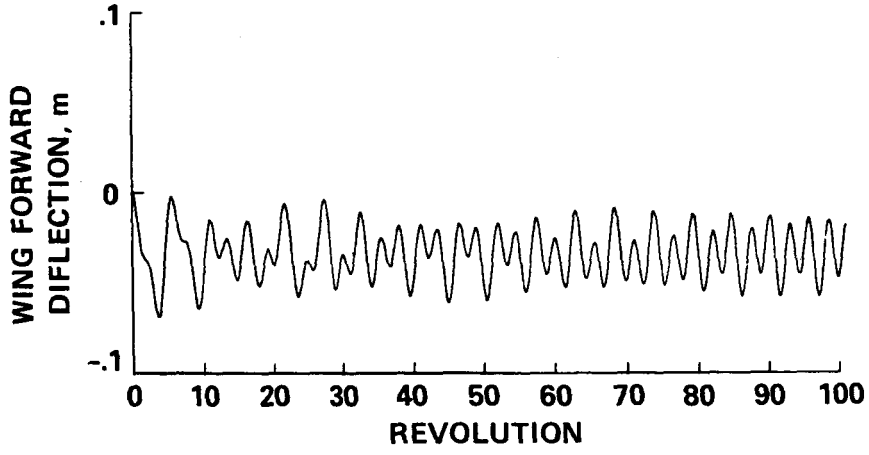

a.- No feedback control.

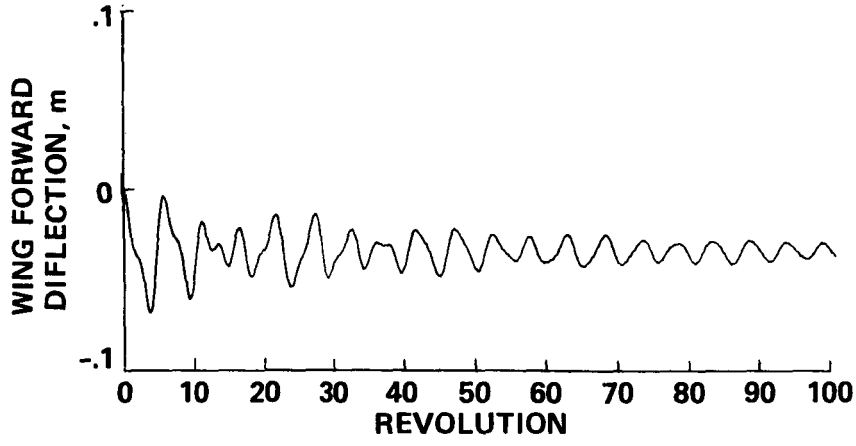

b.- Feedback control; $K_{wcd} = -0.03$.

Figure 20.- Wingtip forward deflection.

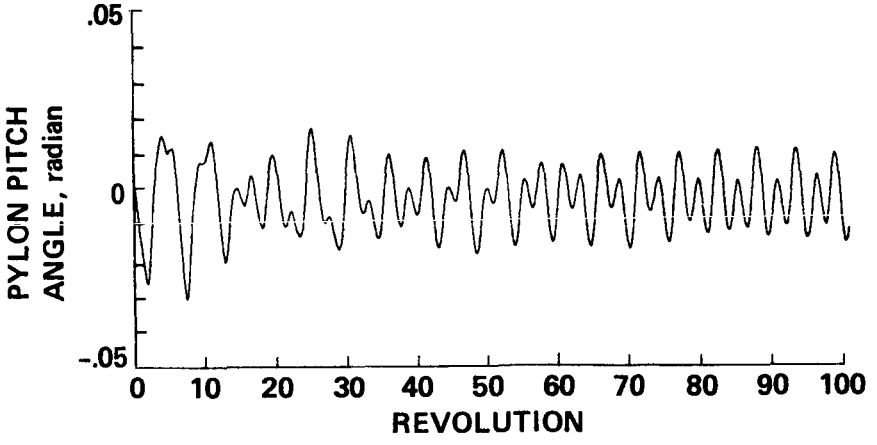

a.- No feedback control.

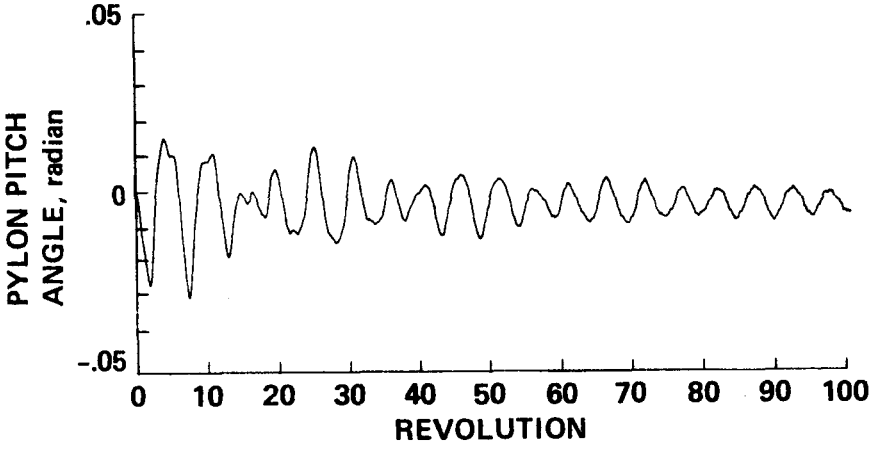

b.- Feedback control; $K_{wcd} = -0.03$.

Figure 21.- Pylon-pitch angle.

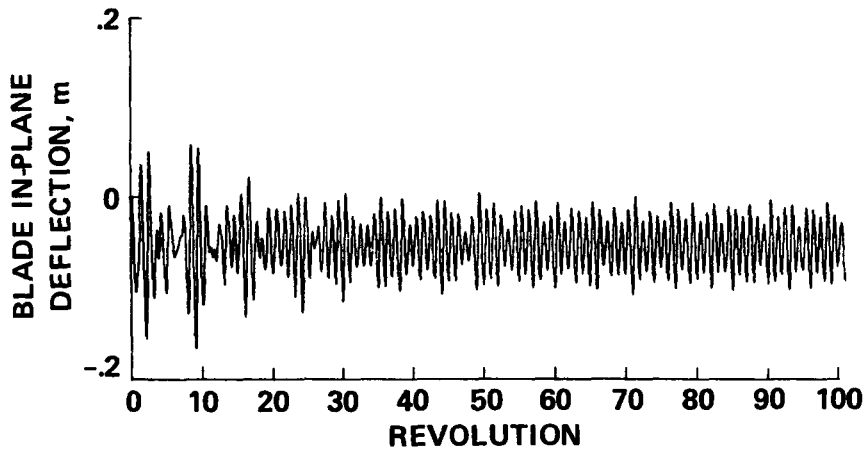

a.- No feedback control.

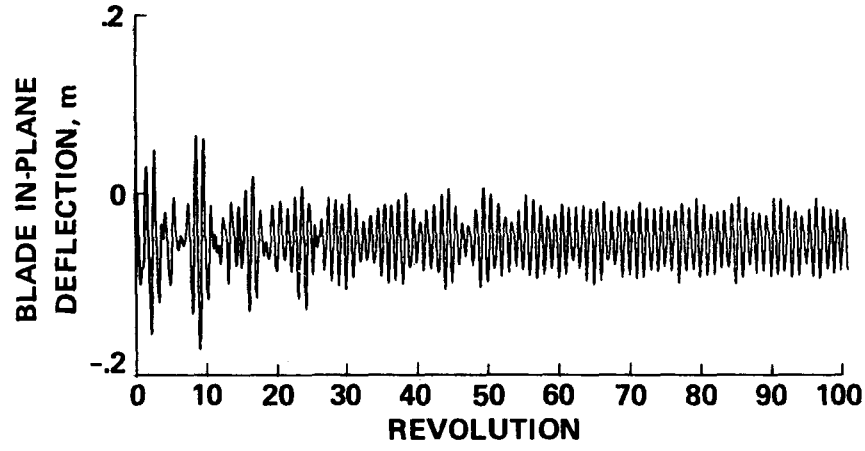

b.- Feedback control; $K_{wcd} = -0.03$.

Figure 22.- First-blade inplane deflection.

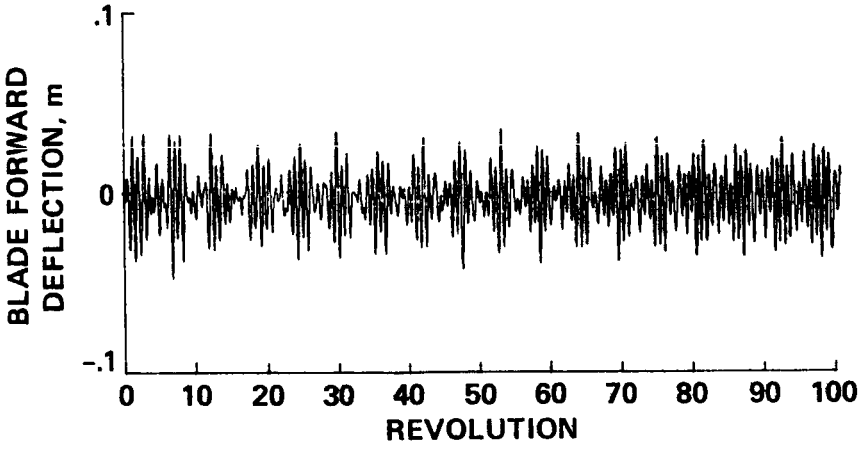

a.- No feedback control.

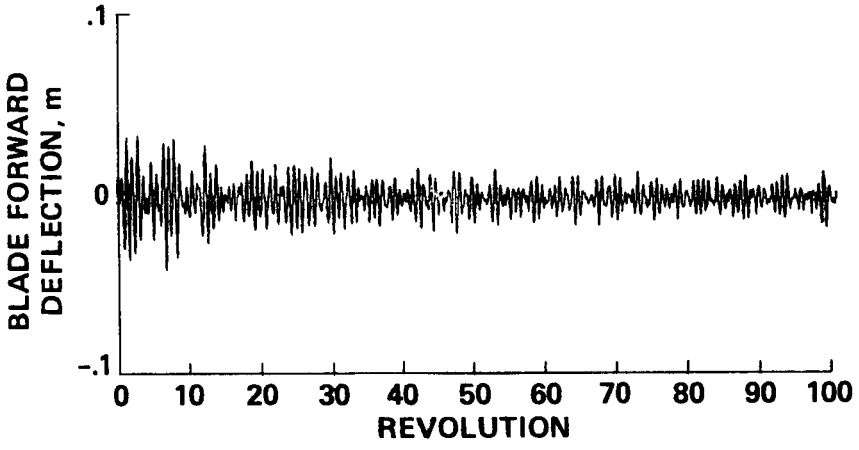

b.- Feedback control; $K_{wcd} = -0.03$.

Figure 23.- First-blade out-of-plane deflection.

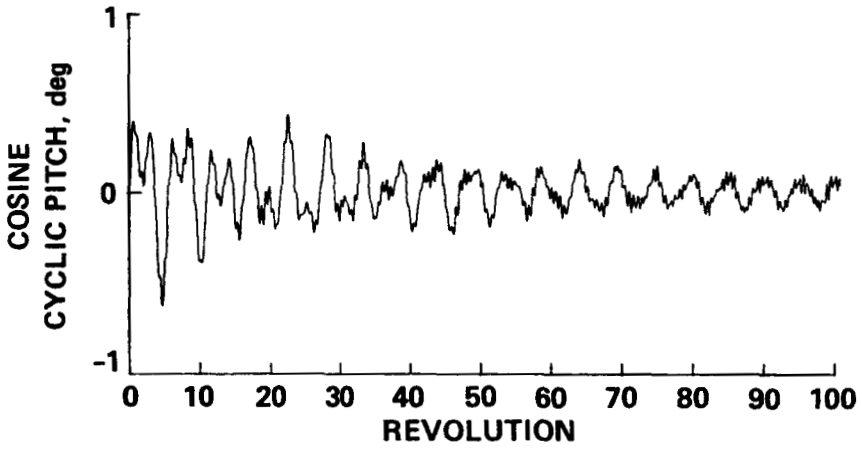

Figure 24.- Cosine cyclic-control pitch used for feedback; $K_{wcd} = -0.03$.

1. Report No.	2. Government Accession No.	3. Recipient's Catalog No.
NASA TM 88315		

4. Title and Subtitle	5. Report Date
TILT-ROTOR FLUTTER CONTROL IN CRUISE FLIGHT	December 1986
	6. Performing Organization Code
7. Author(s)	8. Performing Organization Report No.
Ken-ichi Nasu	A-86286
	10. Work Unit No.
9. Performing Organization Name and Address	11. Contract or Grant No.
Ames Research Center Moffett Field, CA 94035	
	13. Type of Report and Period Covered
12. Sponsoring Agency Name and Address	Technical Memorandum
National Aeronautics and Space Administration Washington, DC 20546	14. Sponsoring Agency Code 505-61-51

15. Supplementary Notes

Point of Contact: Fort Felker, MS 247-1, Ames Research Center, Moffett Field, CA 94035, (415)694-6096 or FTS 464-6096

16. Abstract

Tilt-rotor flutter control under cruising operation is analyzed. The rotor model consists of a straight fixed wing, a pylon attached to the wingtip, and a three-bladed rotor. The wing is cantilevered to the fuselage and is allowed to bend forward and upward. It also has a torsional degree of freedom about the elastic axis. Each rotor blade has two bending degrees of freedom. Feedback of wingtip velocity and acceleration to cyclic pitch is investigated for flutter control, using strip theory and linearized equations of motion. To determine the feedback gain, an eigenvalue analysis is performed. A second, independent, timewise calculation is conducted to evaluate the control law while employing more sophisticated aerodynamics. The effectiveness of flutter control by cyclic pitch change was confirmed.

17. Key Words (Suggested by Author(s))	18. Distribution Statement
Tilt rotor Aeroelastic stability Active control Flutter	Unclassified - Unlimited Star Category - 08

19. Security Classif. (of this report)	20. Security Classif. (of this page)	21. No. of Pages	22. Price*
Unclassified	Unclassified	64	A04

*For sale by the National Technical Information Service, Springfield, Virginia 22161